UNIVERSITY OF GAZİANTEP

GRADUATE SCHOOL OF

NATURAL & APPLIED SCIENCES

MICROSTRUCTURAL ANALYSIS OF PULSE GAS TUNGSTEN ARC WELDING (GTAW) IN Ti-6AL-4V ALLOY

M. Sc.THESIS

IN

MECHANICAL ENGINEERING

by

ALI Shaker Mousa AL-HELLI

FEBRUARY 2013

Microstructural Analysis of Pulse Gas Tungsten Arc Welding (GTAW) In Ti-6Al-4V Alloy

M.Sc. Thesis

In

Mechanical Engineering

University of Gaziantep

Supervisor

Assoc. Prof. Dr. Oğuzhan YILMAZ

by

ALI Shaker Mousa AL-HELLI

February 2013

REPUBLIC OF TURKEY
UNIVERSITY OF GAZİANTEP
GRADUATE SCHOOL OF NATURAL & APPLIED SCIENCES
NAME OF THE DEPARTMENT

Name of the thesis: Microstructural analysis of pulse gas tungsten arc welding (GTAW) in Ti-6AL-4V alloy.

Name of the student: ALI Shaker Mousa AL-HELLI

Exam date: 14.02.2013

Approval of the Graduate School of Natural and Applied Sciences

Assoc.Prof.Dr. Metin BEDİR

Director

I certify that this thesis satisfies all the requirements as a thesis for the degree of Master of Science/Doctor of Philosophy.

Prof. Dr. Sait SÖYLEMEZ

Head of Department

This is to certify that we have read this thesis and that in our consensus/majority opinion it is fully adequate, in scope and quality, as a thesis for the degree of Master of Science/Doctor of Philosophy.

Assoc. Prof. Dr. Oğuzhan YILMAZ

Supervisor

Examining Committee Members

Assoc. Prof. Dr. Okan ÖZER .....

Assoc. Prof. Dr. Oğuzhan YILMAZ .....

Assist. Prof. Dr. A. Tolga BOZDANA .....

I hereby declare that all information in this document has been obtained and presented in accordance with academic rules and ethical conduct. I also declare that, as required by these rules and conduct, I have fully cited and referenced all material and results that are not original to this work.

ALI Shaker Mousa AL-HELLI

ABSTRACT

MICROSTRUCTURAL ANALYSIS OF PULSE GAS TUNGSTEN ARC WELDING (GTAW) IN Ti-6Al-4V ALLOY

ALI Shaker Mousa AL-HELLI M.Sc. in
Mechanical Engineering
Supervisor: Associate Professor Dr. OĞUZHAN YILMAZ

February 2013
68 pages

Aerospace manufacturing industry needs high quality, skilled, accuracy work and reliability manufacturing operations. Tungsten Inert Gas (TIG) welding is one of the welding process methods where it is used effectively in aerospace manufacturing applications. Pulse TIG welding is a part of TIG welding and it is preferred to weld Ti-6AL-4V alloy in order to have sound welding. This work investigates the effects of pulse current TIG welding performance on Ti-6AL-4V. Effects of TIG welding parameters, such as pulse and amperage on material grain size (Gs), heat affected area (HAA) and micro hardness of heat affected zone Mh (HAZ) were analyzed throughout the experiment works. The experimental procedure was carried out according to the design of experiment (DOE) and the results were statistically evaluated by using analysis of variance (ANOVA). Response surface methodology (RMS) was used in evaluating the input factors performance with the responses or outputs and mathematical modeling of TIG welding input parameters for Gs, HAA and Mh (HAZ) were established. Gs is adversely affected by increasing amperage on Ti-6AL-4V alloy. On the other hand, Gs is directly proportional to pulsing. HAA is getting wider with increasing amperage on the contrary HAA is getting narrower when the pulsing increases. Mh HAZ shows a significant increase of hardness with the increasing of pulsing, but inversely reacting with the increasing in amperage.

Key Words: Tungsten inert gas welding, pulse welding, Ti-alloy

ÖZ

DARBELİ GAZ TUNGSTEN KAYNAĞININ Ti-6AL-4V ALAŞIMINDA MİKROTAPİYA OLAN ETKİLERİNİN ANALİZİ

AL-HELLI, Ali Shaker Mousa
Yüksek Lisans Tezi, MakineMühendisliği Bölümü
Tez Yöneticisi Doç.Dr. Oğuzhan YILMAZ

Şubat 2013
68 sayfa

Uzay ve havacılık imalat endüstrisinde, yüksek kaliteli, vasıflı, hassas işler ve üretim operasyonlarında güvenilirlik beklenmektedir. Tungsten asal gaz kaynağı (argon kaynağı) uzay ve havacılık uygulamalarında bu amaca hizmet eden kaynak yöntemlerinden bir tanesidir. Darbeli gaz kaynağı, argon kaynağının bir türüdür ve Ti-6Al-4V alaşımının kusursuz kaynaklanması için tercih edilmektedir. Bu çalışma, darbeli argon kaynağı performansının Ti-6Al-4V alaşımına etkilerini araştırmaktadır. Yapılan deneysel çalışmalarda, tungsten gas kaynağı parametrelerinden darbe ve akım şiddetinin, malzemenin tanecik boyutuna, ısıdan etkilenmiş alanın genişliğine ve ısıdan etkilenmiş alandaki mikro sertlik değerlerine etkileri analiz edilmiştir. Deneyler, deney tasarımı yöntemi ile belirlenmiş ve sonuçlar istatistiksel olarak ANOVA yöntemi değerlendirilmiştir. Girdi ve çıktı ilişki performanslarının değerlendirilmesinde tepkisel yüzey metodolojisi yöntemi kullanılmış ve girdi ve çıktı parametreleri (tanecik boyutu, ısıdan etkilenmiş alan genişliği ve ısıdan etkilenmiş alandaki mikro sertlik) arasında matematiksel modellemeler kurulmuştur. Ti-6Al-4V alaşımında, tanecik büyüklüğü akım gücünün artması ile ters olarak etkilenmektedir. Diğer taraftan, tanecik büyüklüğü darbelenme ile doğru orantılıdır. ısıdan etkilenmiş alanın genişliğine akım şiddetinin artması ile genişler, tam zıt bir biçimde ısıdan etkilenmiş alanın genişliğine darbelenme arttırıldıkça daralır. Isıdan etkilenmiş alandaki mikro sertlik, darbe miktarının arttırılması ile önemli ölçüde artış gösterir fakat akım şiddetinin arttırılması ile ters biçimde karşılık verir.

Anahtar Kelimeler: Tungsten gas kaynağı, darbeli kaynak, Titanyum alaşımı

ACKNOWLEDGEMENTS

The author wishes to express his deepest gratitude to his supervisor Associate Professor Dr. Oğuzhan YILMAZ for his guidance, advice, criticism, encouragements an insight throughout the research.

Secondly, I would like to thank my parents for their great help and motivation during my all education life.

Next I would also like to thank my supportive wife for her fully support during the studies.

Last but not least, I would like to thank my dearest friends Abdulrahman, Hisham, Migi for their supports and advice.

This thesis study was supported by the University of Gaziantep, Scientific Research Project scheme (MF.12.03) Darbeli gaz tungsten kaynağının Ti-6A1-4V alaşımında Mikroyapıya olan etkilerinin Analizi. Yüksek Lisans Araştırma Projesi.

TABLE OF CONTENTS

LIST OF TABLES

Page

LIST OF FIGURES

Page

ABBREVIATION

A…….. Amperage

ANOVA ……. Analysis of Variance

BM……... Base metal

DOE ……. Design of Experiment

FZ…….. Fusion zone

f…… The Jeffries' multiplier

GTAW……... Gas Tungsten Arc Welding

Gs…….. Grains Size

Lc…… Low current

Lp…… Low pulse

Hc…… High current

Hp…… High pulse

HAA…… Heat Affected Area

HAZ……. Heat Affected Zone

Hz……. Unit of Frequency

Mh (HAZ)……. Micro-Hardness of HAZ

N_A……. Numberer of grains per mm^2 at 1X.

N_{Inside}…… Number of Grains Completely Inside the Test Rectangle

$\bar{A}$…… The reciprocal of N_A

$N_{Intercepted}$…… The Number of Grains that Intercept the Test Rectangle

TIG…… Tungsten Inert Gas

CHAPTER 1

INTRODUCTION

1.1 Introduction

Tungsten inert gas (TIG) welding is a process that metals are melting and joining by heating them with an arc occurred between a non-consumable tungsten electrode and the metals, a cylinder of shielding gas is connected to the torch includes the tungsten electrode and one terminal of the power source, the tungsten electrode is in contact with a water-cooled copper tube, the welding current enter the electrode from the power source and the same time preventing overheating as shown in Figure 1.1, the base metal is connected to the other cable of the power source. The shielding gas goes through the torch body and is supplied by a nozzle toward the weld pool to protect it from contamination [1].

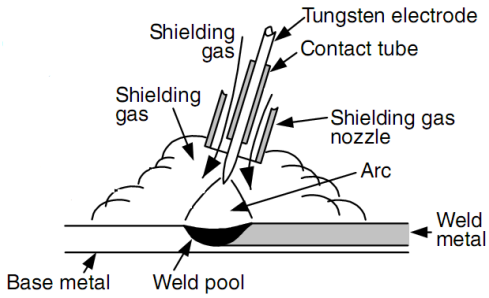

Figure 1.1 Welding area in TIG welding [1]

TIG welding is recommended for joining thin sections because of its limited heat inputs. Welding of thin sheets without addition of filler metals called autogenous welding. It is known that TIG process is a very clean welding process, so that it is used to weld reactive metals, like magnesium, aluminum, titanium and zirconium.

However, TIG welding has low deposition rate. High welding currents can lead to melting of the tungsten electrode and cause brittle tungsten inclusions in the fusion zone [1]. Ti-6AL-4V alloy contains mainly titanium, aluminum (%6), vanadium (%4) and other elements. This alloy is known as difficult to cut materials as well as

difficult to weld since many welding problems such as grain coarsening,hardenability, cracking, porosity etc. can be seen. Therefore, pulse current TIG welding is one of the most popular processes for welding of Ti-6AL-4V alloy in order to prevent these errors and increase welding efficiency.

However, TIG welding process induces changes in the base material and generates unwanted mechanical proprieties and grain formation due to the heat input. The most common way to avoid these problems is using pulse currents that are offering a more uniform heat distribution in the welding area. The pulse TIG welding process has the ability to perform a high quality welding of Ti-6AL-4V alloy with efficiency can be compared with the laser welding process. Therefore, using of pulse current TIG welding is recommended to have good welding quality, mechanical properties and metallurgical properties.

1.2 Scope of thesis

Ti-6Al-4V alloy is widely used in industrial applications like aerospace and aeronautic due to its superior mechanical properties at high temperatures. In this study, considerable experimental works were conducted to examine the pulsing effects on metallurgical properties in order to increase and improve the mechanical properties.

1.3 Objective and aims

The aim of this study is to investigate the effects of the different pulses and currents used in the TIG technique for microstructure characterization of Ti-6Al-4V Alloy. The primary objective of this work is to correlate amperage pulses with microstructure and obtain sound welds using well determined pulses on TIG without welding defects.

1.4 Thesis structure

This thesis starts with an introduction that contains brief information about this research work, the scope and aims to be reached. The literature related to this work was reviewed and discussed in the next chapter. The third chapter is about the experimental setup and the procedure used. In chapter three, DOE, how these

experiments were performed with the explanation of equipment/tools are detailed. Chapter four presents the experiment works and the relationship between factors and responses then discuss the results. Chapter five includes the summary, conclusions and recommendations for future works.

CHAPTER 2

LITERATURE REVIEW

2.1 Introduction

Welding is a method to join materials by the use of heat, force, or a combination of them. Forge welding method was the first process until the end of the 19th century. Then, many welding process had been invented during the early of 20th era to the present day such as Resistance welding, Solid-state welding, Gas welding, Oxyfuel welding, Brazing, Soldering, and Arc welding, which are the main sorts of the welding technology.

Among in all welding process, TIG welding or Gas Tungsten Arc Welding (GTAW) is the most common technology used to weld thin sections of most ferrous and non-ferrous alloys. TIG welding process has greater control, concentrated arc, no slag, no sparks or spatter, little smoke or fumes, and improves weld quality, which ensures good characteristics.

Titanium and its alloys have been one of the prominent engineering metals in many for industrials. Down to its outstanding combination of properties like weight ratio for elevated strength, high toughness, high resistance to corrosion and good fatigue properties, make titanium alloy as eye-catching for many industrial applications particularly aerospace. However, atmospheric contamination effects and grain growth with increasing temperature in fusion welding makes it very difficult. Thus, the researcher and scientist try to improve the TIG welding method and titanium structure itself [2, 3, 4, 5, and 6].

2.2 Related literature

Ti and its alloys are currently welded by different welding processes including TIG welding, Metal inert gas welding (MIG), electron beam (EB) welding, laser beam welding (LBW) and, plasma arc welding (PAW) [5].

Many limitations and restrictions where available in these processes which can negatively affect the metallurgical integrity of the welded joint, and the economic and productivity viability of the process. The welding technique in use for a titanium alloy depends on a number of factors like the alloy itself, the shape and the component size, the level of distortion which can be tolerated in the final product, out-of-position accessibility and properties of the weld microstructures in comparison with the base metal alloy.

At a selected regular frequency, the cycling of the welding current from high to low level involves with argon tungsten pulsed current arc welding which was a variation of TIG welding developed in the 1950s.

The peak current of the high level, in general, is selected to give bead contour and capable penetration, on the other hand, the background current of the lower level is set at a sufficient point to sustain a firm arc [4].

The Inter Pulse TIG welding process has been used to successfully weld titanium alloys, the technique shows that it can substantially decrease the heat input during welding compared to conventional TIG welding, potentially resulting in improved weld macro and microstructures, micro textures and their properties.

The resulting demand further work in this area, which may give in greater understanding of both, phase transformations and mechanical properties in titanium alloy fusion welds and in titanium alloys in general, the effect of pulse on grain refinement shown in Figure 2.1 [2].

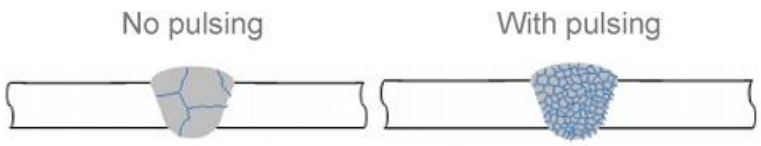

Figure 2.1 The effect of pulse on grain refinement [7]

Demanding the use of improved welding techniques and materials is the way to develop the weld quality related to improvement in process parameters. Alas, titanium alloy welding results of graining coarsening at the heat affected zone and the fusion zone. During welding metal solidification the cause of the prevailing

thermal conditions effects to the weld fusion zone typically displays coarse columnar grains. The statements often results in deficient resistance to hot cracking and deplorable weld mechanical properties [7, 8].

Ti-6Al-4V's welding and its joining technologies have increased substantial attention to apply the alloy to various products. Therefore, the investigation of the fusion welding techniques of Ti-6Al-4V alloy has been conducted by a large number of researchers, particularly in aerospace and chemical activities. As a result of its microstructure can be designed so, it offers a good combination of high fracture toughness and mechanical resistance, additionally, to an excellent corrosion resistance.

When the microstructural characteristics and mechanical properties in laser beam welds of Ti-6Al-4V alloy, the mill-annealed with 5.1mm thickness, were investigated, the fusion zone (FZ) and the heat affected zone (HAZ) which are powerfully influenced by the welding conditions changed obviously after laser beam welding.

The formation of martensite is attributed to strengthen the heat affected zone and fusion zone, while the mechanical properties of the welds are apparently depending on the microstructural characteristics [9, 10].

In both disciplines, pulsed and unpulsed, the fusion zone happened to be closely equated. Although solidification occurred epitaxial, competitive growth in the fusion zone and grain coarsening in the heat affected zone both gives a conclusion of a much wider grain size in the weld metal relative to that of the base material. Severally, in the pulse and unpulsed conditions, the average grain size values of welds were 342μm and 266μm. The modern grain refinement has resulted from the current pulsing. α phase, martensitically to the α′ phase or, a mixture of both, can be taken place diffusional from the breakdown of β grains. It was not attainable to tell the difference between α and α′ phases from the optical micrographs [6, 11].

The formation of martensite is attributed by the strengthening in the fusion zone (FZ) and heat affected zone (HAZ), and the microstructures are mainly being dependent By the hardness distributions in the welds. In the region, because of the increased

amount of ά martensite, the hardness curve quickly ascends, and the creation of ά martensite results in the higher hardness in the partially converted HAZ.

Making to happen in the same hardness in the region, dominant ά martensite within the similar microstructures is configured in the entirely transformed FZ and HAZ. Furthermore, the finer ά martensite structure ascribes the higher hardness of FZ which is provoked by the fastest cooling rate.

The standard tensile elongations and strengths of the welds broadly correspond with those of base metal (BM), and the entire fractures of tensile specimens eventuate at the BM long away from the FZ and HAZ. The tensile test means that the FZ and HAZ are stronger than the BM, which is logically accordant with the hardness test as shown in Figure 2.2 [3, 12].

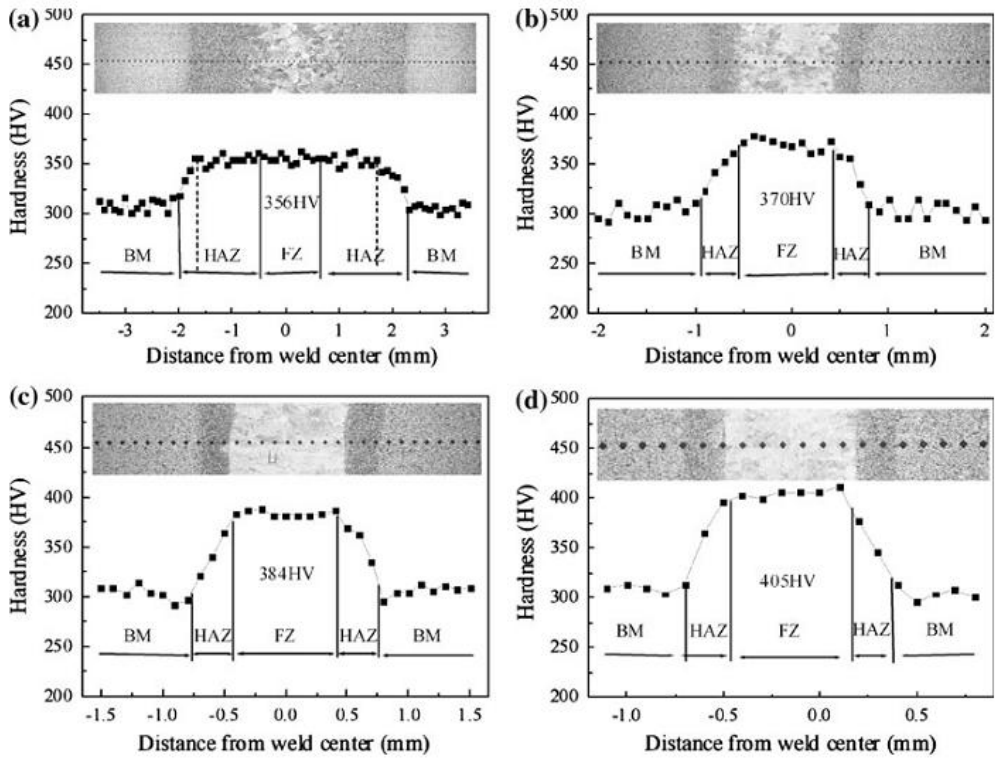

Figure 2.2 Hardness configuration in the center parts of the welds under different welding circumstances: (a) 10 kW and 2 m/min; (b) 10 kW and 4 m/min; (c) 10 kW and 6 m/min; and (d) 10 kW and 8 m/min [3]

Microhardness distributions of workpieces for different average power welded cross-sections by using Vickers micro-hardness tests this literature works analyzed with a load of 300g.

The microhardness test done at 500μm lower than the surface beginning of the center line of the weld pool. As a result, at the center of the weld pool the hardness is at the maximum level and the melted and cooled material is extraordinary compared to the base metal caused by its rapid cooling rate.

The difference in hardness between the weld pool and the base metal is 140HV. In the heat affected zone, heating rises from the weld pool so the hardness is lower than the weld pool and the difference is 84HV.

The difference between the HAZ and the base metal is 56HV, the micro hardness profile across the weldment indicates that the hardness configuration in the fusion zone is higher than both the parent metal and HAZ as shown in figure 2.2 were (a), (b), (c), (d) represents the LB with different parameters. Whereas the increase in average power increases total heat input to the target dropping the cooling rate in addition to the temperature slope [3, 12].

So the hardness is probable to minimize with increasing average power. The high cooling rate related to laser beam welding leads to observed large increase in hardness in laser welded Ti–6Al–4V. The high cooling rates effect on the formation of martensite in the weld zone HAZ region. In addition, Titanium-base materials have reversible transformation properties that crystal structure changes from alpha (hcp, hexagonal close-packed) structure to beta (bcc, body-centered Cubic) structure when the temperatures exceed to a certain level..

Transition temperature is approximately 995^{o}C for Ti-6Al-4V alloy and it is called as "beta tarsus temperature". This allotropic behavior, which depends on the type and amount of alloy contents, allows complex alterations in microstructure and more diverse strengthening opportunities than those of the other nonferrous alloys [13].

Vickers hardness profile of weld friction stir welds Vickers hardness profile across the welds are shown in Figure 2.3, the FZ has a higher hardness value than the BM, and the lowest hardness can be observed in the HAZ [5, 14].

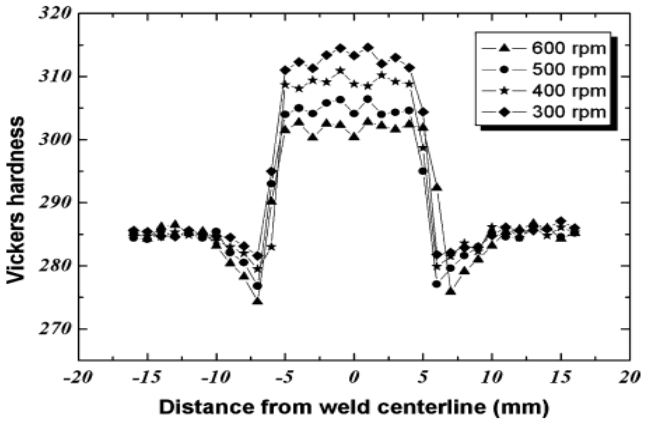

Figure 2.3 Vickers hardness profile across the FZ of the welds produced at different rotational speeds [5]

Generally, the cooling rate effects on laminar α + β phase, the thickness of laminar α + β phase adversely affected by the increasing of cooling rate. And as the cooling rate is relative to the freezing rate, the cooling rate and its amplitude of variation reduce gradually with the increase of freezing time. In a related manner, there is the same law in solid-state phase changes. Therefore increasing the amplitude of lamellar α + β phase with modulus is lesser and lesser [15]

It is obvious that the Vickers hardness decreases with grain size and increasing the smaller the grain size and the thickness of laminar α + β phase, which improve the effects of grain boundary intensity and phase boundary reinforcement. Additionally, the Vickers hardness is positively proportional to the strength of the alloy. As a result, the Vickers hardness decreases by means of grain size and the thickness of laminar α + β phase increasing.

The effects of casting modulus on the grain size, the thickness of lamellar α + β phase, and the Vickers hardness, with the relationships between Vickers hardness, grain size and thickness of lamellar α + β phase were investigated. The literature shows that the greater the modulus, the larger the grain size and the thickness of lamellar α + β phase, and the a smaller amount the Vickers hardness [16].

For Ti-6Al-4V alloy staging casting, the phase transformation from β phase to α+β phase related to solid-state phase change and the new phases are formed by

nucleating and growing. With the increase of cooling rate, the increase of nucleation ratio, however the decrease of diffusion, the new phases are difficult to grow up. Therefore, the smaller the modulus of specimens, the greater the cooling rate, and the less the thickness of laminar α+β phase formed in solid-state phase changes of Ti-6Al-4V alloy. The researchers selected grains and α+β phases as many as possible to calculate their average value in order To reduce experimental error [16].

The phase relationships show that the quantity of β phase will increase during heating, completely transforming to β at α temperature of 956°C. Higher than this temperature, the β phase is stable up to the solidus temperature of 1693°C, as complete melting occurs at the liquidus temperature of 1701°C, These temperatures are slightly different than those published elsewhere based on experimental measurements, where the liquids are reported to be 1655°C, the solidus to be 1605°C, and the β transits to be 975°C. [17]

Weld Microstructure; the fusion zone FZ is characterized by the shape of large columnar grains that solidified as β and subsequently underwent a near complete transition to a finely dispersed α or ά phase. The ά phase is a martensitic phase with similar lattice parameters to α phase and an hcp crystal structure [17].

During welding cooling in the HAZ, the β→α transformation initiated at the β transus temperature, but completed the transformation below the Ms Temperature. The transition from β→α to β→ά appeared to take place after approximately 5-10% of the microstructure had initially transformed into an in both the partially transformed and the completely transformed regions of the HAZ [17].

In α+β titanium alloys, the morphological characteristics of the acicular α–β structure can be modified by varying the cooling rate after β processing. Specifically, displacive transformation of β can form structures such as α′ martensite at high cooling rates, while at lower cooling rates; the diffusional transformation (nucleation and growth) of β gives a Widmanstätten α–β structure.

It is important to note that the morphology and size of α colony in titanium alloys have an important influence on various mechanical properties, including tensile strength, ductility, fracture toughness and fatigue strength. It has been reported that by decreasing α colony size through suitable thermo mechanical processing

procedures, the yield strength, ductility and fatigue crack nucleation resistance are improved [6, 18].

Poor welds metal ductility of tungsten inert gas (TIG) welded Ti–6Al–4V has been attributed to larger β grain size and high heat input. On the other hand, poor ductility and toughness of electron beam (EB) welded Ti–6Al–4V has been attributed to the α′ martensitic structure in the weld metal due to higher cooling rates [6].

The optical microscopy is considered not as an exact method of studying the, α and β phases in Ti-6Al-4V, as a result of the non-uniform etching response of their phase. The severely etched locations could be considered as β and the lightly etched locations could be considered as α.

The laser beam welded joints resulted in a small aspect ratio and increased hardness due to the short period of exposure to the laser heat input and followed by rapid quenching. The microhardness increases from the parent metal to the fusion zone along the transverse direction.

The Vickers microhardness test showed a reduction in hardness in the fusion zone of weldments fabricated by TIG welding. This is attributed to the annealing effect caused by the multi pass welding process. Whereas the Vickers hardness value of the LBW was very high when compared TIG welding, due to the rapid heating and quenching action [19].

Peak current, background current, pulse frequency and pulse on-time are the predominant Factors which are having a greater influence on fusion zone grain refinement of pulsed current gas tungsten arc welding process. It involves cycles of the welding current from a high level to a low level at a selected regular frequency. The high level of the peak current is generally selected to give adequate penetration and bead contour, while the low level of the background current is set at a level sufficient to maintain a stable arc. This allows arc energy to be used efficiently to fuse a spot of controlled dimensions in a short time producing.

Recently, considerable research has been performed on pulsed current gas tungsten arc welding process and reported advantages include improved bead contour, lower

heat input requirements, reduced residual stresses and distortion. The consequence of the thermal fluctuations leads to periodic interruption in the process of solidification.

As the pulse current decays, the solid liquid interface advances in towards the arc and increasingly becomes vulnerable to any disturbances in the arc form. As a result, if peak current is less than 60 A, then incomplete penetration and lack of fusion have been observed. At the same time, if peak current is greater than 100 A, then undercut and spatter has been observed on the weld bead surface.

If background current is lower than 20 A, then the arc length is found to be very short. On the other hand, if the background current is greater than 60 A, then arc becomes unstable and arc wandering is observed due to increased arc length. If a pulse frequency is 0 Hz, then the bead appearance and bead contours appear to be similar to those of constant current weld beads.

Further, if pulse frequency is greater than 12 Hz, then more arcs Spatter has been experienced. If pulse on time is lower than 35%, then weld nugget formation is not so smooth due to incomplete melting of base metal. On the contrary, if the pulse on time is greater than 55%, then over melting of base metal has been noticed [8].

At high peak current values the molten pool is agitated more resulting in grain refinement in the weld region, in turn, resulting in increased hardness and refinement in grain size. Metallography studies showed that welds where most brittle parts of welded joint with the coarsest grains and highest micro hardness. The hardness in the fusion zone in the as welded condition was found to be increased, which is to be ascribed to the large prior beta grain size.

These results are consistent with the microstructural observations that a refined microstructure is associated with a higher hardness optimum pulse frequency at which grain refinement is optimum leading to increase in hardness. Thus there exists an optimum frequency at which greatest effect is produced. In the current investigation, the frequency of 6 Hz resulted in maximum grain refinement [20].

Mechanical and thermal disturbances to the weld pool at very low frequency of pulsing are expected to be less intense leaving no effect on the weld pool. At high frequencies, the vibration amplitude and temperature oscillation induced on the weld

pool is reduced to a greater extent almost leading to continuous current, resulting in reduced effect on the weld pool [20].

After performing a large number of trial runs using 1.6 mm thick mill annealed sheets of titanium Ti–6Al–4V alloy, the feasible working limits of pulsed TIG welding parameters were identified as shown in Table 1.1.

Table 1.1 Welding factors and their levels [4]

				Levels coded				
SI No.	Factor	Notation	Unit	(−2)	(−1)	(0)	(+1)	(+2)
1	Peak current	P	A	60	70	80	90	100
2	Base current	B	A	20	30	40	50	60
3	Pulse frequency	F	Hz	0	3	6	9	12
4	Pulse-on-time	T	S	35%	40%	45%	50%	55%

Hence, in this investigation an attempt was made to develop mathematical models to predict the grain size and hardness of argon tungsten pulse current arc welded titanium alloy using statistical tools such as design of experiments, analysis of variance and regression analysis [4].

Basically, gas tungsten arc welding is strongly characterized by the weld pool geometry. This is because the weld pool geometry plays an important role in determining the mechanical properties of the weld. On the other hand, it is widely understood that the TIG welding of titanium alloy exhibits columnar grains in the weld pool, which often results in inferior mechanical properties and may lead to hot cracking. The current pulsing technique was attempted by many researchers to great success, resulting in grain refinement of fusion zone, Selection of process parameters in TIG welding of 1.6 mm titanium alloy was presented for obtaining the optimum grain size and hardness [21].

Unlike the usual current welding, in pulsed TIG heat energy is supplied only during peak current pulses allowing it to dissipate into the base metal during the background current and thus lowering heat buildup in the adjacent base material, this can lead to a narrower heat affected zone. Pulsed TIG has secured a niche for itself in applications such as welding of root passes of tubes and welding thin sheets, where

precise control over penetration and heat input are required to avoid burn through [20].

Pulsed current tungsten inert gas welding is a variation of continuous current tungsten inert gas welding that involves cycling the welding current at a selected regular frequency. The maximum current is selected to give adequate penetration and bead contour, while the minimum is set at a level sufficient to maintain a stable arc.

In contrast to constant current welding, in pulsed TIG heat energy is supplied only during peak current pulses, allowing it to dissipate into the base metal during the background current and thus lowering heat buildup in the adjacent base material, thus leading to a narrower heat-affected zone. Advantages include improved bead contours, greater tolerance to heat sink variations, lower heat input requirements, reduced residual stresses and distortion, refinement of fusion zone microstructure, and reduced the width of HAZ [21, 22].

Welding of titanium alloy leads to grain coarsening at the fusion zone and heat affected zone (HAZ), Weld fusion zones typically exhibit coarse columnar grains as a result of the prevailing thermal conditions during welding metal solidification.

This often results in inferior weld mechanical properties and poor resistance to hot cracking. It is thus highly desirable to control solidification structure in welds and such control is often very difficult as a result of higher temperatures and higher thermal gradients in welds in relation to castings and the epitaxial nature of the growth process, Nevertheless, several methods for refining weld fusion zones have been tried with some success in the past: inoculation with heterogeneous nucleates microcooler additions, and surface nucleation induced by gas impingement and introduction of physical disturbance through techniques such as torch vibration.

In this literature, two relatively new techniques namely, magnetic arc oscillation and current pulsing, have gained wide popularity as a result of their striking promise and the relative ease with which these techniques can be applied to actual industrial situations with only minor medications of the existing welding equipment [4].

In this literature an attempt has been made to develop mathematical models to predict the grain size and hardness of argon tungsten pulse current arc welded

titanium alloy weldments. Four factors, five level, central composite, rotatable design matrix are used to optimize the required number of experiments. The mathematical models were developed by response surface method (RSM). The adequacy of the models was checked by ANOVA technique. By using the developed mathematical models, grain size and hardness of the joints can be predicted with 99% confidence level [4].

Welding of thin sections of Ti–6Al–4V was accomplished by Single pass gas tungsten arc welding with pulsing current technique, the result found to be better to a conventional continuous current process in terms of grain refinement in the fusion zone [20].

The short period of arc provided by pulse current allows the energy to efficiently to fuse a spot of controlled dimensions producing the weld as a series of overlapping nuggets and limits the wastage of heat by conduction into the adjacent parent material as in normal constant current welding. In contrast to constant current welding, the heat is dissipated into the base material leading to a narrower heat affected zone (HAZ), because the fact that heat energy required to melt the base material is supplied only during peak current pulses for short intervals of time. [4].

The semi-automatic and automatic welding equipment could be applied to Pulsed current TIG welding and that has great advantages like avoiding weld cracks, improving arc stability, reducing thermal distortion, and reducing residual stresses by means of reduction of the total heat input [23, 24].

Compared to conventional gas tungsten arc welding, The Inter Pulse technique uses magnetic constriction and high frequency modulation of the arc current (20,000Hz) to seriously reduce the overall heat input , In titanium alloys, the α to β phase transformation, which occurs according to the Burgers orientation relationship and that gives microtexture characterization takes on particular importance [25].

An Inter Pulse 150 narrow bead manual TIG precision welding system was used to produce in 1.2mm thick Ti-6Al-4V and Cp-Ti sheet. Welding parameters typically consisted of average current of 20-40A, an arc voltage of 9V, the use of different welding parameters had a considerable effect on the overall microstructures and textures in different welds [25].

The TIG welding was done manually; the frequency of the TIG was kept constant as 6 HZ. The weld bead, quality of weld and full penetration was achieved by selecting suitable welding parameters, the microstructural examinations of the weldments were done using an optical microscope, The polished specimens were etched with Krolls reagent (1 to 3mlHF, 2 to 6mlHNO and 100mlH O, as ASTM192).

The microhardness examinations were carried out using 0.5 kg load, HAZ is broad in TIG welding due to the high heat input, the slow cooling or annealing process minimizes the martensite formation. On observing the microstructures it is possible that, a higher hardness value would be a sign of the presence of a hard microstructure and vice versa. In this literature the martensite structures (dark) are of higher hardness and the alpha (light) has poorer hardness [19].

TIG welding is The preferred welding process for titanium alloys, due to its improved economy and comparatively easier applicability. In the case of a single-pass TIG welding of a thinner section of this alloy, the pulsed current has been found advantageous due to its advantages over the conventional continuous current process.

Since titanium is very chemically reactive at high temperatures, welding of titanium alloys is difficult. During welding, titanium alloys easily pick up oxygen and nitrogen from the atmosphere, over the past decades; many new titanium-based materials have been developed for different ranges of application. It is generally understood that the the characteristics of the microstructure effected very much on mechanical properties of titanium alloys. The types of phase, grain size and grain shape and the distribution of fine microstructures determine the properties and, therefore, the application of titanium alloys [26].

Weld fusion zones in general show coarse columnar grains as a result of the prevailing thermal conditions through welding metal solidification. This frequently results in inferior weld mechanical properties and poor resistance to hot cracking. It is thus highly desirable to Solidification structure in welds and such control is often very difficult because of higher temperatures and higher thermal gradients in welds in relation to castings and the epitaxial nature of the growth process Pulsed-current TIG welding involves the cycling of the welding current from a high level to a low level at a selected standard frequency.

The high level of the peak current is generally selected to give an adequate penetration and bead contour, while the low level of the background current is set at a level sufficient for maintaining a stable arc. This permits arc energy to be used efficiently to fuse a spot of controlled dimensions in a short time, producing the weld as a series of overlapping weld beads and limiting the wastage of heat by conduction into the adjacent parent material as in normal constant current welding [26].

Current pulsing has been used by several investigators to obtain grain refinement in Weld fusion zones and improvement in weld mechanical properties, however, the reported research work on relating the pulsed current parameters and mechanical properties are very scarce. The trial runs were carried out using 1.6 mm-thick rolled sheets of titanium Ti-6Al-4V alloy to find out the feasible working limits of the pulsed-current TIG welding parameters. Procedure (without filler metal addition) was followed to fabricate the joints.

The toughness and strength could be negatively effected by Welding of this alloy as a result of thermal cycles to which it is exposed. Therefore highly attractive to control solidification structure in welds and such control is often very difficult as a result of higher thermal gradients and higher temperatures in welds in relation to castings and the epitaxial nature of the growth process.

In pulsed current welding, during peak current the heat energy supplied to melt the base material and that occurs in a short period of interval and this permits the heat to scatter quickly into the (BM) the result is a narrower HAZ. The technique has secured a niche for itself in specific applications for example in the welding of welding thin sheets, and in root passes of tubes, where precise control more penetration and heat input are required to stay away from burning through [27].

Weld fusion zones normally show evidence of coarse columnar grains as a result of the existing of thermal conditions during welding metal solidification. This regularly results in poor resistance to hot cracking and inferior weld mechanical properties. Although it is thus highly advantageous to manage the solidification structure in welds, such control is often very difficult, as a result of the elevated thermal gradients and higher temperatures in welds in relation to castings and the epitaxial nature of the growth process [28].

The use of improved welding techniques and materials led to develop the weld quality and that associated with improvement in process parameters. Nevertheless, a number of methods for refining weld fusion zones have been tried with some success in the past: Inoculation with heterogeneous nucleants, microcooler additions, and surface nucleation induced by gas impingement and introduction of physical disturbance through techniques for example torch vibration and pulsed current welding. The grain refinement in weld fusion zones and improvement in weld mechanical properties obtained by Current pulsing that few investigators where working on it [28, 11]

Most of the published articles give attention to the effect of pulsed current welding on tensile properties and grain refinement infusion zone microstructure. Thus, in this study; an effort has been made to find out the effects of pulsing on HAZ [28].

On the other hand, the weld pool is agitated turbulent, at high pulse frequencies, because of severe arc and results in surplus heat input which Be the result of coarse grain formation in the fusion zone. At the optimized pulse frequencies, the weld pool oscillation and arc vibration are now adequate to cause more nucleation sites and make possible the fine grain formation [28].

Changing in weld pool solidification conditions lead to refining the fusion zone microstructure this opportunity done by Pulse current TIG welding. Figure 2.4. In pulsed current TIG welding, arc current changing with time as a square wave, Metallurgical advantages of pulsed current welding often reported in the literature contain refinement of fusion zone grain size and substructure, reduced width of the heat affected zone, control of segregation, etc. All these factors help in enhancing the mechanical properties of welding [6].

As a result, in the previous works, the researchers didn't use a wide range of pulses current and analysis their effect on grain size, microhardness and width of heat affected zone HAZ, moreover there is no serious study about the effect of changing pulse on the width of heat affected zone HAZ.

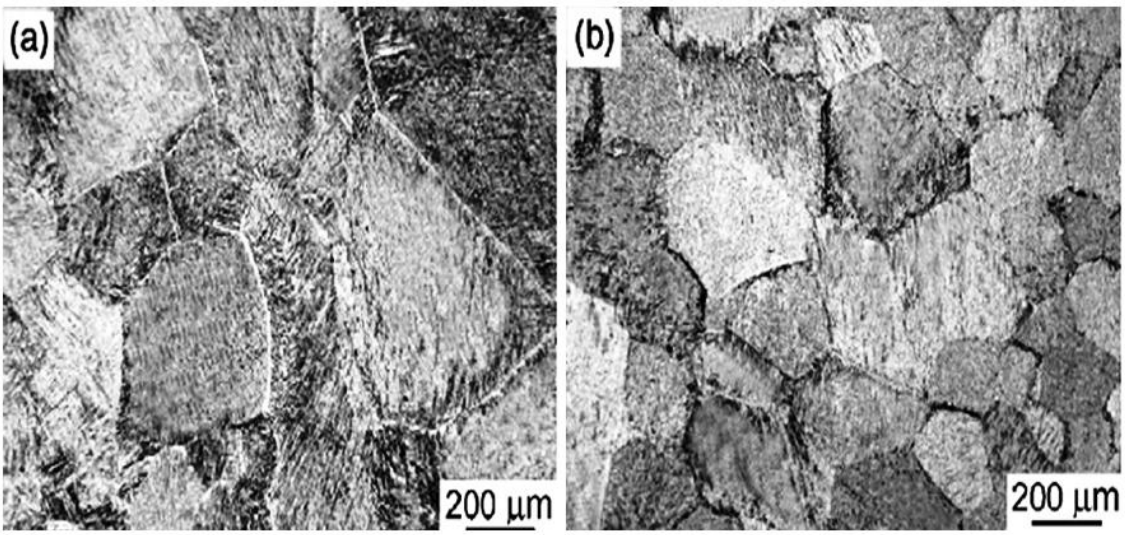

Figure 2.4 Optical microstructures of weld metal in the as-welded condition; (a) unpulsed, (b) pulsed [6]

2.3 Literature gaps

After reviewing the related literature, it has been noticed that using pulses in TIG welding are very effective obtaining sound and defect-free welds. Almost in all the works which used pulses in TIG welding implemented 0-12 Hz. In fact, today's TIG welding machines are capable of supplying 0-20,000 Hz intervals including some specifically developed machines. Thus, there is almost no work which focuses on using high pulse intervals in TIG welding of Ti-6Al-4V alloys and investigates their effect on the grain size number, microhardness and width of the heat affected area.

CHAPTER 3

EXPERIMENTAL SET-UP AND PROCEDURE

3.1 Introduction

In the present chapter, the experimental works and the procedure that was followed during the welding operations as well as equipment and their properties are given in detail.

3.2 Experimental set-up

3.2.1 Welding procedure

The TIG welding applications were performed manually by LINCOLN V320-T AC/DC welding machine, An ordinary power supply connected straight polarity (DCSP), is used for TIG welding of titanium as shown in Figure 3.1. The machine's minimum and maximum currents are 5-320A, and pulse frequency is between 0-2500 Hz. The welding machine torch is a link torch (lt 18 w) water cooled duty cycle 100%, 1.8 cm cup size with 2% thoriated tungsten. The tungsten electrode distance from the tip point till the ceramic cup is between 4-9 mm. The ground tungsten electrode tip was taken not exceed 2-1/2 of electrode diameter and the grinding direction horizontally of the grinding wheel.

A good control of heat input can be achieved by pulsed TIG welding. The current supplied from a DC Power source with pulses have a predetermined duration of the low and peak values. The required penetration for welding will take place when the current is maintained at the high on-position. The torch is manipulated to correct the positioning, during the off-position. To keep the arc not extinguished, the ionized column is retained and the electrode is kept sufficiently hot. With low heat input to the joint, deep penetration could be obtained in this process. The porosity is minimized and agitates the molten weld metal by the pulse arc. [29].

Arc stiffness is one of the results of pulsing and also avoiding arc fluctuate is another advantage. Cracking and burn-through in the molten weld pool can be avoided by well manipulated and successive solidification of the nuggets, the mechanical properties and the grain structure improved with low heat input of the weld as well. There is no need for weaving because the pulsed current is adequate to melt the desired base metal area. For the root run of the tube and pipe welding Pulsed TIG welding is convenient [29].

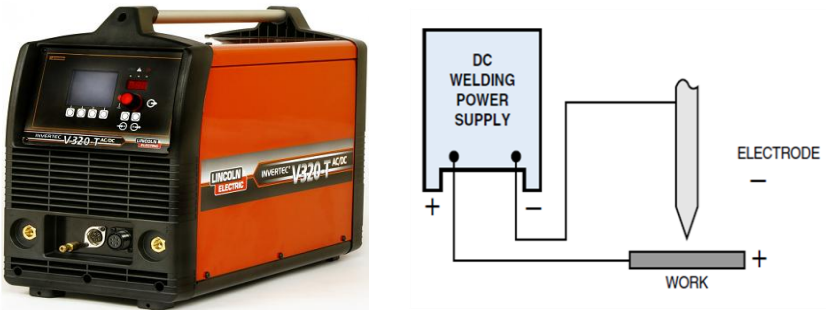

Figure 3.1 Welding machine with straight polarity (DCSP)

In mechanized TIG and During joining specific parts by pulsed TIG, rapid current rise and the current decrease with a high pulse repetition rate is used. The usefulness of pulsed TIG are; difference in joint fit-up can be tolerated, less skill Operator required , Welding of sheets down to 1 mm thickness can be achieved, Mechanization is possible, less Distortion , more control of welding Position , perfect for critical applications like dissimilar metals joining, and root passes of pipes, etc. [29].

The same weld as a standard arc in pulse TIG welding process could be produced but with much less heat input and that is one of the main advantages of the pulsed TIG welding. Penetration is rapidly achieved As peak amperage is reached, the amperage is reduced to the point where the pool is allowed to cool but current is sufficient to keep the arc established, before the workpiece can become heat saturated [30].

With pulse arc the need to control heat input as the weld progresses is greatly reduced, the pool is more control when welding is out of position, and in cases where joints are of different thicknesses the welder will have more controllable welding in Figure 3.2.

Peak Amperage: this value is usually set slightly higher than it would be set for normal TIG weld. Background Amperage: this certainly would be set less than the peak amperage. Pulses per Second: is the number of times per second that the weld current reaches peak amperage, and "% On Time" is the pulse peak period as a percentage of total time. It controls how long the peak amperage level is maintained before it drops to the background value [30]

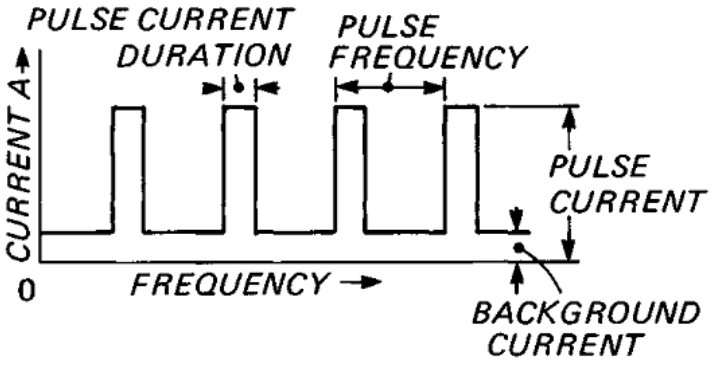

Figure 3.2 Pulse current parameters [30]

Titanium welding needs a clean environment in order to have good welding. Isolate an area, specific welding zone for the welding of titanium, helps to make quality welds. This area should be preserved clean and should keep it away from dirt produced by operations such as painting, torch cutting and grinding. Moreover, the humidity should be controlled and working site should be free of air drafts [31].

When welding with the GTAW process and titanium the cleanliness of the weld joint area is an important circumstance. Grease, oil, paint shop dirt, marking crayon, and corrosion deposits or rust all must be taken away from the metal surfaces and joint edges to a distance farther than the heat affected zone, the presence of these dirt during welding may result in contaminated welds and arc instability. The weld bead could have a pore, inclusions or cracks, if the weld made with any of these contaminants exists [31].

From where the weld bead is to be made on both sides of the specimens, an area of (25mm) 1 inch should be cleaned. The joint edges should be brushed with a stainless steel wire brush and greased with non-chlorinated solvents such as acetone, using a clean lint-free cloths or cellulose sponges, is acceptable, provided no residue remains [31].

The properties and corrosion resistance of titanium weld metal will degrade due to inclusion of these foreign substances in the fusion zone. In critical cases, cleaning by acid may be desired. The specimen's surfaces usually require only abrasion with normal cleaners, followed by washing with hot water then air drying. In order to provide no residue remains, wiping of weld joints and adjacent areas with non-chlorinated solvents such as toluene or acetone, using a clean lint-free cloths or cellulose sponges, is reasonable. With a view to removing traces of oil and grease the solvents are particularly effective for this operation, after using solvent cleaning it should be followed by stainless steel wire brushing, should not use steel brushes or steel wool on titanium by no means because of the hazard to corrosion resistance which embedded iron particles pose [31].

In this work the main parameters were current and pulse, the current (40-80) A and pulse (0-2500) Hz. The welding time depends on the current; low current long time high current short time. Experimental works were conducted by dividing those two parameter intervals in two groups;

Group (1): low current (40, 50, 60A) and low pulse (0, 500, 1000Hz);

Group (2): high current (60, 70, 80A), high pulse (1500, 200, 2500Hz).

Argon gas was used as shielding gas and its flow rate was 20 liter per minute. The welding position was horizontal. A trailing shield box was used as shown in Figure 3.3. A sample of specimens in welded position is shown in Figure 3.4

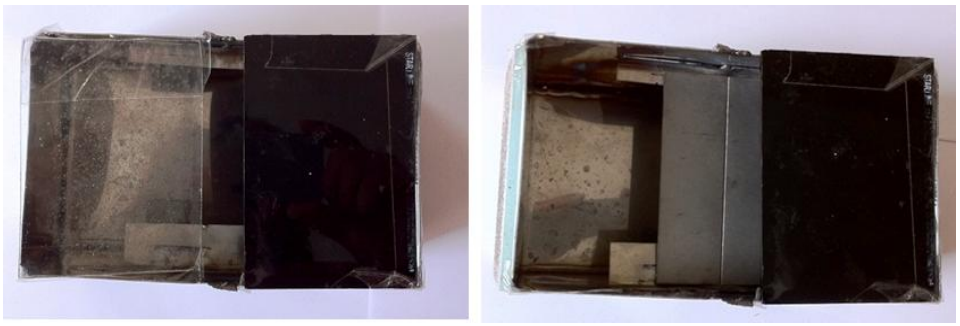

Figure 3.3 A trailing shield box Dimensions; 10 cm width, 18 cm length, 10 cm height.

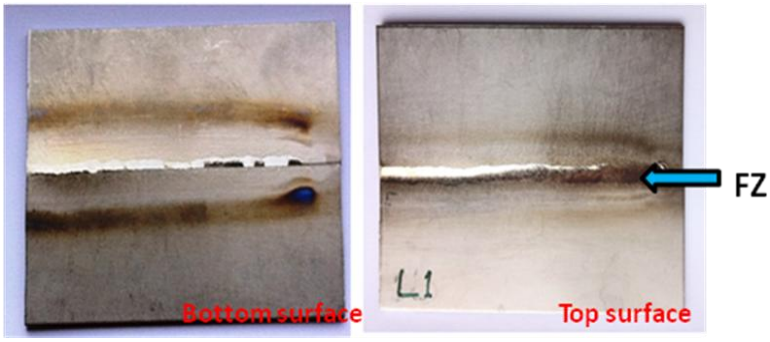

Figure 3.4 Welded specimens

3.2.2 Specimens

Ti-6Al-4V is one of the most widely used titanium alloys. This alloy is used in the aerospace industry, pressure vessels, aircraft gas turbine disks, cases and compressor blades, and medical industry. Ti-6Al-4V has a good combination of strength and toughness along with good corrosion resistance. The properties of this alloy are developed by relying on the refinement of the grains upon cooling from the beta region, or the alpha-plus-beta region, and subsequent low-temperature aging to decompose martensite formed upon quenching. When this alloy is slowly cooled from the beta region, alpha begins to form below the beta transus, which is about 980 °C (1796 °F) [32].

Welding alpha-beta alloys can significantly change their strength, ductility, and toughness characteristics as a result of the thermal cycle to which they are exposed. Alpha-beta alloys, such as Ti-6Al-4V and other weakly beta-stabilized alloys can be joined successfully in the annealed condition or in the solution-treated and partially aged condition, with aging completed during the postweld stress-relief heat treatment. Low ductility results from welding of many alpha-beta alloys. The low ductility of most alpha-beta alloy welds is caused by phase transformations [32].

The specimen dimensions are 90 mm length, 30 mm width, and 1.5 mm thickness as shown in Figure 3.5. Two pieces were used to join by welding. Two sets of specimens were prepared (thirteen in each), one first set was for low current (Lc) and the second set was for high current (Hc), as shown in Tables 3.1 and 3.2.

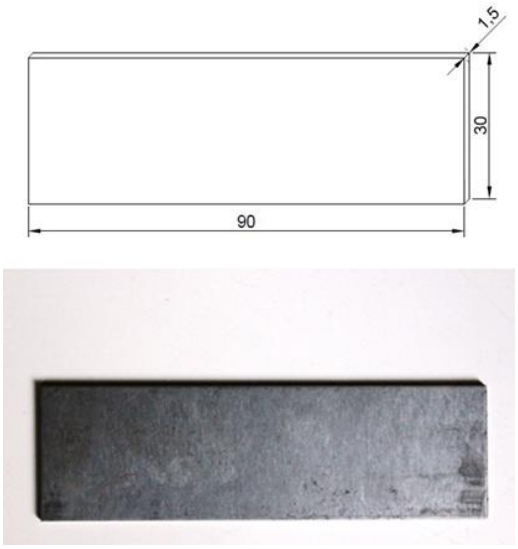

Figure 3.5 Specimen dimensions

After welding, the specimens were cut to specific dimensions, such as 10 mm width and 30 mm length in order to be suitable for mounting machine cylinder diameter.

Table 3.1 Experimental work sheet for Low current (Lc) and Low pulse (Lp)

Specimens	**Parameters**	
	Lc (A)	**Lp (Hz)**
L1	40	1000
L2	60	500
L3	50	500
L4	40	500
L5	50	0
L6	50	500
L7	60	1000
L8	40	0
L9	50	500
L10	50	500
L11	60	0
L12	50	1000
L13	50	500

Table 3.2 Experimental work sheet for High current (Hc) and High pulse (Hp)

Specimens	Parameters	
	Hc (A)	Hp (Hz)
H1	60	1500
H2	70	2000
H3	80	2500
H4	60	2500
H5	80	2000
H6	70	2500
H7	60	2000
H8	80	1500
H9	70	2000
H10	70	2000
H11	70	1500
H12	70	2000
H13	70	2000

3.2.2 Specimen Preparations: Mounting, Grinding and Polishing

Mounting is a process to cover materials which have non-uniform geometries or small size in order to observe specimens under microscope. Mainly thermoset materials such as Bakelite, Lucite, and epoxy resins are used with the aid of die pressure machines as shown in Figure 3.6. The cylinder diameter of the machine is 38 mm and the specimen has the same as the cylinder as shown in Figure 3.7. The selection of the mounting medium depends upon equipment available, specimen size, and the metallographies features of interest.

Figure 3.6 Bakelite mounting machine

bakelite is recommended when edge preservation is important. Nickel plating specimens before mounting assists in edge preservation, by adding 50 Vol% of silica (SiO_2) or similar hard material powder, between 200 - 325 mesh, to the epoxy resin mounting material. When the metallographies examination involves the hybrid phase it would be better to leave the specimen unmounted or to mount it in a room-temperature-setting epoxy resin, because of the increased solubility of hydrogen in titanium at only moderately increased temperatures [33]. In this work, Bakelite was used as mounting materials due to its availability and properties that are explained above.

Grinding procedure of titanium alloys is similar to that for grinding steel specimens. The specimens that were prepared in this work were ground on successive grades of silicon carbide papers, starting with 180-grit and proceeding to 240-, 400-, and 600-grit papers, using water keeping the specimens cool and to flush away loose particles of metal and abrasive.

Figure 3.7 Sample specimens mounted in Bakelite

It is possible to start grinding with a paper as coarse as 80 grit. Hand, disk, and belt grinding should be used [33].

Manual polishing consists of three stages: rough, intermediate, and final polishing. The rough polishing is accomplished on a high-speed polishing wheel covered with a lintless rayon or silk cloth as shown in Figure 3.8, using medium pressure and levigated 1- or 3-μm α-alumina (Al_2O_3). The levigated Al_2O_3 is placed on the wheel and wetted with water or an acid solution if an etching action is desired. It may also first be mixed with the desired reagent, acid, or water and applied to the wheel as slurry [33].

A typical 500 ml slurry may contain 15 g levigated Al_2O_3, 10 ml nitric acid (HNO_3), 1.5 ml hydrofluoric acid (HF), with the balance consisting of water. An alternative rough polishing technique is the use of a nylon cloth and a 15 to 6μn diamond paste [33]. In this work, two stages of polishing (intermediate and final) were performed since limestone powder was chosen as polishing powder which gives better results for titanium alloys. Also, green Al_2O_3 was used with acetone media.

Figure 3.8 Polishing machine

Several cycles of polishing and etching may be needed to remove smeared metal. Etching should be light to avoid pitting. The specimen is unetched when final polishing begins. The specimen is held in position on the polishing wheel with the edge to be maintained as shown in Figure 3.9. The mount specimen was rotated in place about 30 to 40° to minimize streaking the mount specimen surface [33].

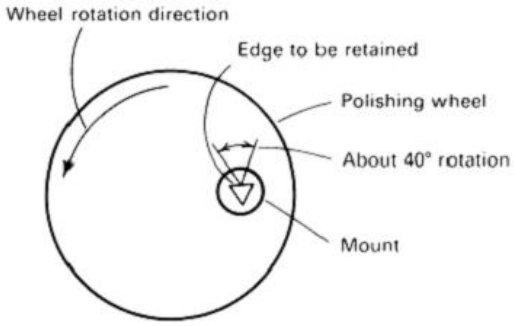

Figure 3.9 Specimen and polishing wheel set-up to improve edge retention in Ti-6AL-4V [33]

Etching several etchants is used for macroetching and microetching of titanium and titanium alloys as shown in Figure 3.10. Macroetching is usually performed by immersion. Microetching is accomplished by swabbing or immersion

Etching times are usually short, ranging from 30-35 seconds under microscope. The specimen should be examined after light etching to avoid over etching. Nearly all etchants for titanium and titanium alloys contain HF and an oxidizing agent, such as HNO3. Kroll's reagent, a dilute aqueous solution containing HF and HNO3, is the etchant most widely used for commercial titanium alloys (Distilled water 92 ml-Nitric Acid 6 ml-HF Acid 2 ml) [33].

Figure 3.10 Etching solution for Ti-6AL-4V

3.2.4 Grain Size Measurement

It is known that the mechanical properties like strength, ductility, and toughness were directly affected by the Grain size. In the present work different pulses current used to try to more understand this behaviour. Grain refinement is the set of technique used to implement grain boundary strengthening in metallurgy. The specific

techniques and corresponding mechanisms will vary based on what materials are being considered.

The test method of determination of average grain size in metallic materials ASTM E112 – 10 STANDARD is chief measuring procedures and, for the reason that of their merely geometric basis, is self-governing of the metal or alloy concerned. In fact, the essential procedures may also be used for the evaluation of average grain, crystal, or cell size in nonmetallic materials [34].

Planimetric (or Jeffries') procedure in the planimetric procedure draws a circle or rectangle of known area (regularly 5000 mm² to make simpler the calculations) on a micrograph, a monitor or on the ground- glass screen of the metallography. Choose a magnification which will give at least 50 grains in the field to be counted. When the image is focused properly, counts the number of grains in this area. The calculation of all the grains included completely within the known area plus one half the numbers of grains intersected by the circumference of the area gives the number of equivalent entire grains, measured at the magnification used, within the area. If this number is multiplied by the Jeffries' multiplier, *f*, the result will be the number of grains per square millimeter N_A. Count a minimum of three fields to ensure a sensible average. The number of grains per square millimeter at 1X, N_A, is calculated from:

$$N_A = f\left(N_{inside} + \frac{N_{intercepted}}{2}\right) \quad (3.1)$$

$$f = M^2 / \text{Area of shape} \quad (3.2)$$

$$G = (3.321928 \log 10 N_A) - 2.954 \quad (3.3)$$

M is the magnification, where *f* is the Jeffries' multiplier; N Inside is the number of grains completely inside the test circle and $N_{\text{Intercepted}}$ is the number of grains that intercept the test circle.

The ASTM grain size number, *G*, can be calculated from N_A (number of grains per mm² at 1X) using equation (3.3), N_A in mm², the average grain area, $\bar{A}$, is the inverse of N_A, that is, 1/ N_A then compare the result in Table 3.3.

Grain size (Gs) used from this table is N_A Grains/mm² at 1X and to find the exact number of Gs linear interpolation used. The area of the test is rectangular and it was 2.257398316 mm² [34].

Olympus optical microscope with 100X magnification was used as well as image processing a Scopephoto 3.0 program, Digital Camera for Microscope replaces one of the microscope eyepieces (Figure 3.11).

Figure 3.11 Olympus optical microscope

For each specimen more than one picture was taken and the average of the grain number to area is used to calculate the Gs as shown in Figures 3.12, 3.14, and appendix A. The digital camera program Scopephoto scale needs a criterion, so micro ruler used to regulate the scale Olympus optical microscope as shown in Figure 3.13.

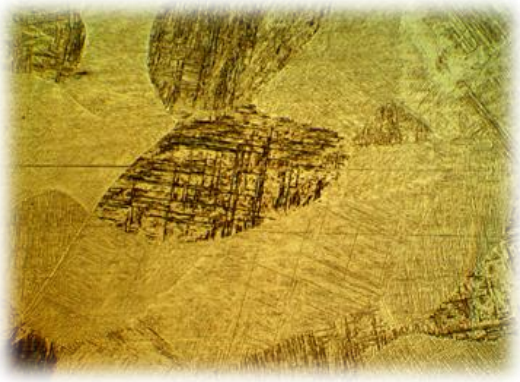

Figure 3.12 Specimen H12 with 100X magnification

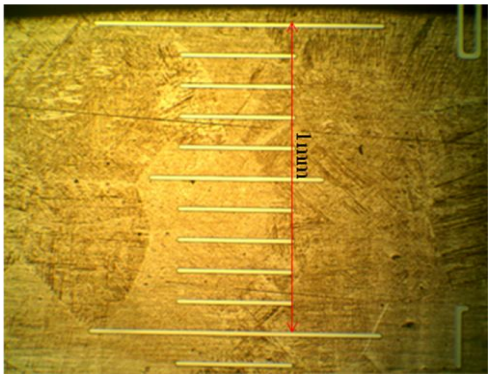

Figure 3.13 Micro ruler

Table 3.3 Grain Size Relationships Computed for Uniform, Randomly Oriented, Equiaxed Grains [34]

Grain Size No. G	$\bar{N}_A$ Grains/Unit Area		$\bar{A}$ Average Grain Area		$\bar{d}$ Average Diameter		$\bar{\ell}$ Mean Intercept		$\bar{N}_L$
	No./in.^{2} at 100X	No./mm^2 at 1X	mm^2	μm^2	mm	μm	mm	μm	No./mm
00	0.25	3.88	0.2581	258064	0.5080	508.0	0.4525	452.5	2.21
0	0.50	7.75	0.1290	129032	0.3592	359.2	0.3200	320.0	3.12
0.5	0.71	10.96	0.0912	91239	0.3021	302.1	0.2691	269.1	3.72
1.0	1.00	15.50	0.0645	64516	0.2540	254.0	0.2263	226.3	4.42
1.5	1.41	21.92	0.0456	45620	0.2136	213.6	0.1903	190.3	5.26
2.0	2.00	31.00	0.0323	32258	0.1796	179.6	0.1600	160.0	6.25
2.5	2.83	43.84	0.0228	22810	0.1510	151.0	0.1345	134.5	7.43
3.0	4.00	62.00	0.0161	16129	0.1270	127.0	0.1131	113.1	8.84
3.5	5.66	87.68	0.0114	11405	0.1068	106.8	0.0951	95.1	10.51
4.0	8.00	124.00	0.00806	8065	0.0898	89.8	0.0800	80.0	12.50
4.5	11.31	175.36	0.00570	5703	0.0755	75.5	0.0673	67.3	14.87
5.0	16.00	248.00	0.00403	4032	0.0635	63.5	0.0566	56.6	17.68
5.5	22.63	350.73	0.00285	2851	0.0534	53.4	0.0476	47.6	21.02
6.0	32.00	496.00	0.00202	2016	0.0449	44.9	0.0400	40.0	25.00
6.5	45.25	701.45	0.00143	1426	0.0378	37.8	0.0336	33.6	29.73
7.0	64.00	992.00	0.00101	1008	0.0318	31.8	0.0283	28.3	35.36
7.5	90.51	1402.9	0.00071	713	0.0267	26.7	0.0238	23.8	42.04
8.0	128.00	1984.0	0.00050	504	0.0225	22.5	0.0200	20.0	50.00
8.5	181.02	2805.8	0.00036	356	0.0189	18.9	0.0168	16.8	59.46
9.0	256.00	3968.0	0.00025	252	0.0159	15.9	0.0141	14.1	70.71
9.5	362.04	5611.6	0.00018	178	0.0133	13.3	0.0119	11.9	84.09
10.0	512.00	7936.0	0.00013	126	0.0112	11.2	0.0100	10.0	100.0
10.5	724.08	11223.2	0.000089	89.1	0.0094	9.4	0.0084	8.4	118.9
11.0	1024.00	15872.0	0.000063	63.0	0.0079	7.9	0.0071	7.1	141.4
11.5	1448.15	22446.4	0.000045	44.6	0.0067	6.7	0.0060	5.9	168.2
12.0	2048.00	31744.1	0.000032	31.5	0.0056	5.6	0.0050	5.0	200.0
12.5	2896.31	44892.9	0.000022	22.3	0.0047	4.7	0.0042	4.2	237.8
13.0	4096.00	63488.1	0.000016	15.8	0.0040	4.0	0.0035	3.5	282.8
13.5	5792.62	89785.8	0.000011	11.1	0.0033	3.3	0.0030	3.0	336.4
14.0	8192.00	126976.3	0.000008	7.9	0.0028	2.8	0.0025	2.5	400.0

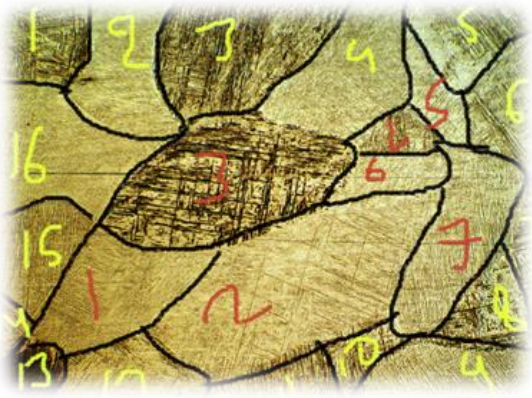

Figure 3.14 Grains number counting with 100X magnification

3.2.5 Width of HAZ measurement

The heat-affected zone describes the area of a metal that is altered during welding. The metals in the HAZ typically melt slightly. To determine HAZ, its must plug values into a mathematical formula. The voltage, current, and efficiency should be known. Concentrated processes that use limited heat typically result in a low HAZ while general processes that use a high amount of heat typically result in a high HAZ. The heat affected area HAA measurement took by Nikon microscope as shown in Figure 3.15

Figure 3.15 Nikon microscope

There is no such a direct calculation or ready-made formula available to calculate the width of the HAZ, generally the width of HAZ depends on several factors.

- Welding Process used,
- Welding parameters / Heat input used,
- Preheat / Interpass temperatures,
- Material and Thickness used, etc.

In Figure 3.16 a specimen HAA size measured by Nikon microscope in mm.

Figure 3.16 HAA width size

3.2.6 Microhardness test

Hardness could be referred in a sort of ways, as indicated by the names of the tests that indentation tests: A pyramid, cone or ball is applied onto the surface of the tested metal. The relationship of the area to the load or depth of indentation is the measure of hardness, like in Rockwell, Brinell, Vickers, and Knoop hardness tests [35].

In this study Leitz microhardness device used to measure the micro hardness of Ti-6AL-4V alloy as shown in Figure 3.17. The indentation test position was in the horizontal middle line in the specimen, the average of micro hardness indentation point value used for each region in the FZ and HAZ as shown in Figure 3.18.

The estimated results from micro-hardness device calibrated with Table 3.4 to find the hardness magnitude. The micro hardness testing time was 30 second, and the measuring took it as compare with the chart the weight was 200 g.

Figure 3.17 Leitz micro-hardness device

Table 3.4 Micro-hardness measure comparison with 200g weight

d in μ	Vickershärte HV									
	0	1	2	3	4	5	6	7	8	9
19	1027	1017	1006	996	985	975	965	955	946	937
20	927	918	909	900	891	883	874	866	857	849
21	841	833	825	817	810	802	795	788	780	773
22	766	759	753	746	739	733	726	720	713	707
23	701	695	689	683	677	672	666	660	655	649
24	644	639	633	628	623	618	613	608	603	598
25	593	589	584	579	575	570	566	562	557	553
26	549	544	540	536	532	528	524	520	516	512
27	509	505	501	498	494	490	487	483	480	476
28	473	470	466	463	460	457	453	450	447	444
29	441	438	435	432	429	426	423	420	418	415
30	412	409	407	404	401	399	396	394	391	388
31	386	383	381	379	376	374	371	369	367	364
32	362	360	358	355	353	351	349	347	345	343
33	341	339	336	334	332	330	329	327	325	323
34	321	319	317	315	313	312	310	308	306	304
35	303	301	299	298	296	294	293	291	289	288
36	286	285	283	281	280	278	277	275	274	272
37	271	269	268	267	265	264	262	261	260	258
38	257	255	254	253	252	250	249	248	246	245
39	244	243	241	240	239	238	237	235	234	233
40	232	231	229	228	227	226	225	224	223	222
41	221	220	218	217	216	215	214	213	212	211
42	210	209	208	207	206	205	204	203	202	202
43	201	200	199	198	197	196	195	194	193	192
44	192	191	190	189	188	187	186	186	185	184
45	183	182	182	181	180	179	178	178	177	176
46	175	175	174	173	172	172	171	170	169	169
47	168	167	166	166	165	164	164	163	162	162
48	161	160	160	159	158	158	157	156	156	155
49	154	154	153	153	152	151	151	150	150	149
50	148	148	147	147	146	145	145	144	144	143
51	143	142	141	141	140	140	139	139	138	138
52	137	137	136	136	135	135	134	134	133	133
53	132	132	131	131	130	130	129	129	128	128
54	127	127	126	126	125	125	124	124	124	123
55	123	122	122	121	121	120	120	120	119	119
56	118	118	117	117	117	116	116	115	115	115
57	114	114	113	113	113	112	112	111	111	111
58	110	110	109	109	109	108	108	108	107	107
59	107	106	106	105	105	105	104	104	104	103
60	103	103	102	102	102	101	101	101	100	100

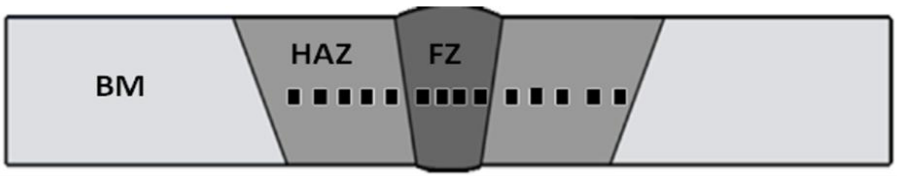

Figure 3.18 Indentations measuring points in the specimen

3.3 Design of experiments (DOE)

Minitab program (Minitab 16)® had been used for the design of experiment (DOE) in this study. Minitab provides four categories of designing experiments: factorial, response surface, Taguchi, and mixture, Response surface method (RSM) used in these works. In order to check the relationship between one or more response variables, Response surface method used for a set of quantitative experimental

variables or factors, In this work there are two factors and three responses. These methods are often put to use after the experiment have identified a controllable factor, to optimize the response, the factory settings should be found. Designs of this type are usually chosen when you suspect curvature in the response surface [36].

Response surface methods could be used in :

- Find operating conditions (factor settings) that create the best response.
- Find factor settings that satisfy process specifications or operating.
- Recognize new operating conditions that produce established improvement in product quality over the quality accomplished by current conditions.
- Model a correlation between the response and the quantitative factors.

3.3.1 Creating an Experimental Design

Before entering or analyze measurement data in Minitab®, it must first create an experimental design and store it in the worksheet. Relying on the necessities of study experiment, it possible to select from an assortment of designs. Minitab® helps researcher to select a design by providing a list of all the existing designs. Minitab® automatically creates the design and stores it in the worksheet after choosing the design and its features, [36].

The purpose of using the Response surface design is to study the relationship between two factors, packing procedure and, order processing system, and the time it takes to prepare an order for shipping.

Starting File then new, afterwards choose Minitab Project. Chose OK. Or, just start Minitab, then Stat ➢ DOE ➢ Response surface ➢ Create RS Design. When design created in Minitab, at the start only two buttons are available, Display Available Designs and Designs. The other buttons are enabled after you complete the Designs subdialog box. Then Display Available Designs. For most design types, Minitab displays all the achievable designs and the number of required runs in the Display Available Designs dialog box, by clicking OK to return to the main dialog box. Under Type of Design, choose central composite, 2 factors (default generators), In Number of factors, choose 2, then Designs. The box at the top shows all available designs for the design type and the number of factors. Number of center point ➢

default, value of alpha ➢ face centered, number of replication ➢ 1, to return to the main dialog box then OK.

3.3.2 Name factors and set factor levels

Minitab enters the names and levels you enter for each factor into the worksheet and uses the names as the labels for the factors on the analysis output and graphs. If you do not enter factor levels, Minitab sets the lower level at –1 and highest level at 1.

From Factors, Click the cube points in the levels defines. Then change the factor name by double clicking: Factor A, type current in Name's Column, type 40 in low for current and 60 in high, Factor B, type pulse in Name's Column, type 0 in low for pulse and 1000 in high. Click OK to return to the main dialog box.

By default, Minitab randomizes the running order of all design types, except Taguchi designs. Randomization helps to make certain that the model meets certain statistical assumptions and can also help decrease the effects of factors not included in the study.to ensure you obtain the same running order every time you create the design, Setting the base for the random data generator.

Then, Options ➢ In Base for random data generated, type 9 ➢ OK in each dialog box ➢ result.

After you conduct the experiment and collect the data, you can enter the data into the worksheet. The characteristic you measure is called a response.

In the Data window, click the column name cell of C7 and type Gs, click the column name cell of C8 and type HAA width, and click the column name cell of C9 and type Mh (HAZ).

Now the design created and the response data collected, you can fit a model to the data and generate graphs to evaluate the effects.

3.3.3 Analyzing the Design

Minitab enables the DOE after it RSM menu commands Analyze RSM Design and RSM Plots, in order to created and stored a factorial design. At this point, the work could be fit a model or generate plots, depending on the design..

To find the main Effect plot, start ➤ ANOVA ➤ main Effect plot, for response choose Gs,and for factors choose Lp, Lc.

In order to find Regression this procedure had been followed:

Starts ➤ Regression ➤ for response choose Gs, predictors choose Lc, Lp.

CHAPTER 4

RESULTS AND DISCUSSION

4.1 Introduction

In this chapter, the results of experiments and the discussions about the presented results are given.

4.2 Experimental works

This study includes twenty six experiments with different parameters offered by Design of experiment (DOE) Response surface design in the Minitab statistical program. The experiments were divided into two groups as shown in Table 4.1 and 4.2.

In this research work, two different input parameters: (1) current and (2) pulse and three output parameters: (1) grain size number, (2) heat affected zone width and (3) microhardness for heat affected zone (HAZ) were considered.

Table 4.1 Experimental work sheet for Low current (Lc) and Low pulse (Lp)

No.	**Run order**	**Input**	
		Lc (A)	**Lp (Hz)**
1	1	40	1000
2	2	60	500
3	3	50	500
4	4	40	500
5	5	50	0
6	6	50	500
7	7	60	1000
8	8	40	0
9	9	50	500
10	10	50	500
11	11	60	0
12	12	50	1000
13	13	50	500

Table 4.2 Experimental work sheet for high current (Hc) and high pulse (Hp)

No.	Run order	Input	
		Hc (A)	Hp (Hz)
1	1	60	1500
2	2	70	2000
3	3	80	2500
4	4	60	2500
5	5	80	2000
6	6	70	2500
7	7	60	2000
8	8	80	1500
9	9	70	2000
10	10	70	2000
11	11	70	1500
12	12	70	2000
13	13	70	2000

Table 4.3 Experimental results for Lc and Lp of Gs, HAA and Mh (HAZ)

NO	Run order	Inputs		Outputs		
		Lc (A)	Lp (Hz)	Gs (number)	HAA (mm)	Mh (HAZ) VHN
1	1	40	1000	78740.8	7.800	386
2	2	60	500	42420.9	12.198	351
3	3	50	500	58281.4	11.362	364
4	4	40	500	69799.5	9.825	371
5	5	50	0	49284.6	11.308	358
6	6	50	500	51810.3	11.530	362
7	7	60	1000	42526.1	11.604	355
8	8	40	0	62372.3	10.445	367
9	9	50	500	56310.3	11.710	362
10	10	50	500	54078.9	11.393	367
11	11	60	0	36004.3	12.494	347
12	12	50	1000	62372.3	10.971	379
13	13	50	500	56310.3	11.686	369

Depending on the Minitab work sheet the experiments done for the outputs Gs, HAA, and Mh (HAZ) and the resulting data arranged in works sheet as shown in Tables 4.3 and 4.4.

Table 4.4 Experimental results for Hc, Hp of Gs, HAA and Mh (HAZ)

NO	Run order	Inputs		Outputs		
		Hc	Hp	Gs	HAA	Mh (HAZ)
1	1	60	1500	60401	11.491	360
2	2	70	2000	71798	10.612	371
3	3	80	2500	93579	10.364	391
4	4	60	2500	12444	10.175	376
5	5	80	2000	54116	11.253	383
6	6	70	2500	105628	10.286	379
7	7	60	2000	71903	11.075	371
8	8	80	1500	44366	11.703	379
9	9	70	2000	67275	10.510	369
10	10	70	2000	66907	10.737	374
11	11	70	1500	53819	11.399	367
12	12	70	2000	67117	10.655	367
13	13	70	2000	66938	10.646	376

4.3 ANOVA Experiments test

Analyses of variance (ANOVA) a statistical analysis tool that separates the total variability found within a data set into two components: random and systematic factors. The random factors do not have any statistical influence on the given data set, while the systematic factors do. The ANOVA test is used to determine the impact independent variables have on the dependent variable in a regression analysis. Interaction plot and main effect plot are used as ANOVA tools to show how factors will react with different responses.

A main effect is an outcome that is a consistent difference between levels of a factor. The main effects plots simply show the average outcome for each value or each variety, combining the effects of the other variables is if all variables were different. On the other hand, interaction plots illustrate the effects between variables which are not independent.

4.3.1 Effects of TIG welding input parameters on Gs

In both, low pulses and high pulses a visible effect of pulse on the grain size, the grains numbers increasing with the increasing of pulses as shown in Figures 4.1, and 4.2. The increasing in the pulse has the greater effect on the grain size as noticed at the highest pulsing where the grains keeping their increase

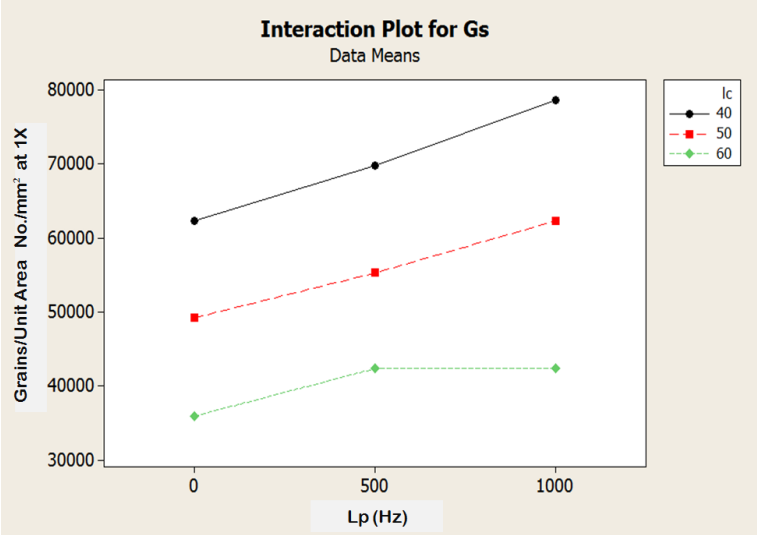

Figure 4.1 Interaction plot of Lp for Gs

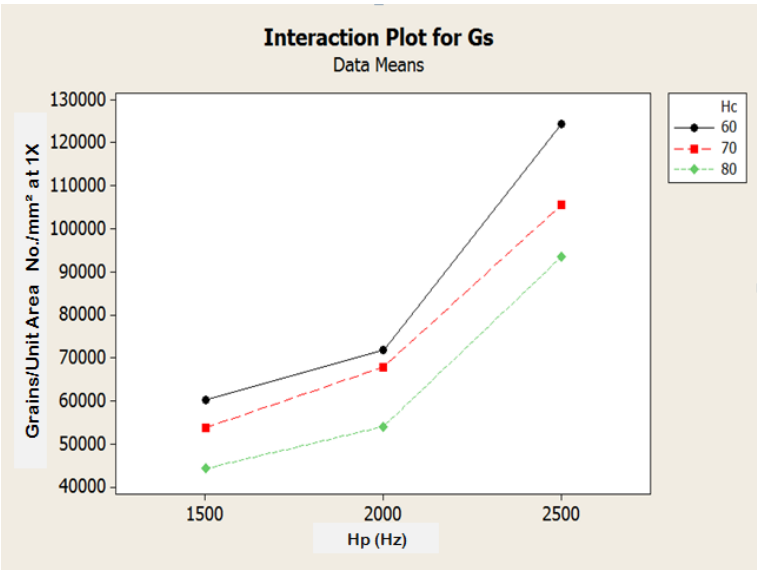

Figure 4.2 Interaction plot of Hp for Gs

Welding of Ti-6AL-4V alloy leads to grain coarsening at the fusion and heat affected zone, this often results in inferior weld mechanical properties and poor resistance to hot cracking. Pulsed current in TIG welding has remarkable effects on grains

refinements, where the increasing of pulses accompanied with decreasing of grain size that means increasing of grains per unit area.

These results are consistent with the microstructure observations that a refined microstructure is associated with a higher hardness. At high peak current sets the molten pool is agitated gives more grain refinement in the weld region. These results are consistent with the microstructure observations that a refined microstructure is associated with a higher hardness.

The energy required for slip or a crack to travel in metal with finer grains are higher compared to that in metal with coarse grains, because the grain boundaries acts as barriers. In The grain boundary strengthening the grain boundaries act as pinning points impeding further dislocation propagation Grain refinement was accompanied by an increase in hardness, ultimate tensile strength, and tensile ductility.

Pulsing enhances fluid flow, reduces the temperature gradient, and causes a continual change in the weld pool size and shape resulting in refinement of microstructure and in turn has resulted in enhanced mechanical properties. The hardness decreased with increasing grain size, increasing of grains leads to increasing of boundaries.

The main effects plot (Figures 4.3 and 4.4), shows how the grain size related to changing with current and pulse. Where the increasing in the current accompanied by decreasing in the grain size while the increasing in the pulse affected positively and increase the grain per unit area.

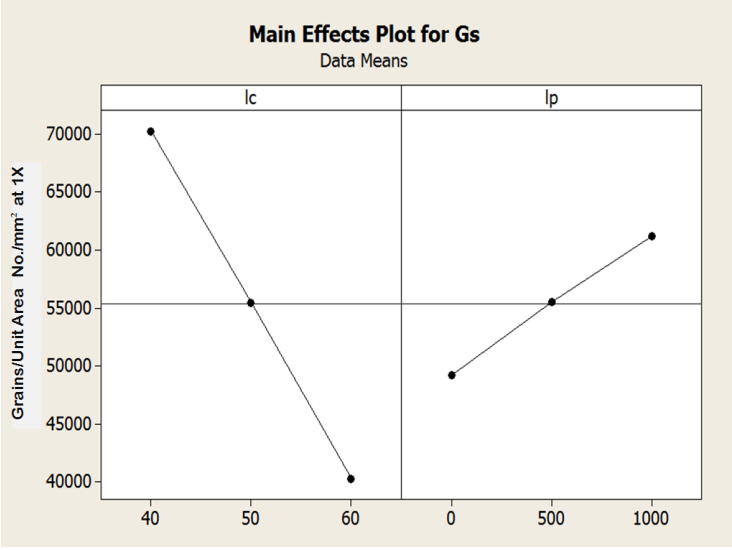

Figure 4.3 Main effects plot of Lc, Lp for Gs

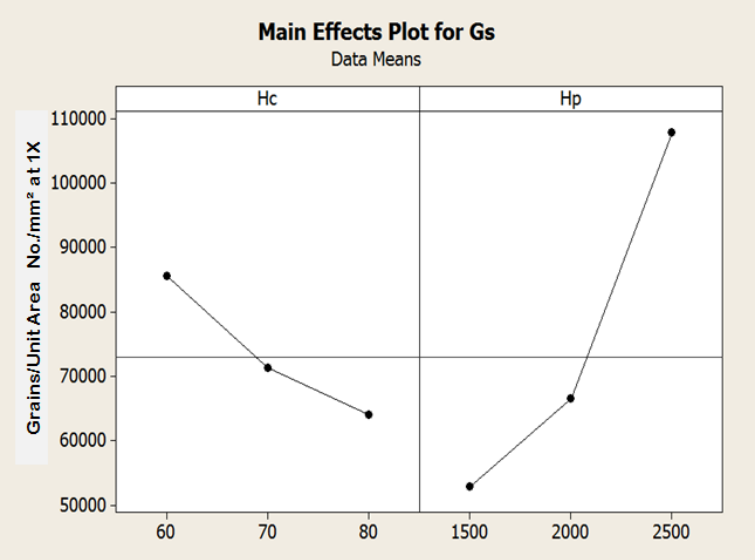

Figure 4.4 Main effects plot of Hc, Hp for Gs

4.3.2 Effects of TIG welding input parameters on HAA

In both, low pulses and high pulses a visible effect of pulse on the heat affected area, the HAA decreases with the increasing of pulses at variance to current that shows a wider HAA whenever it increased as shown in Figures 4.5, 4.6, 4.7, and 4.8.

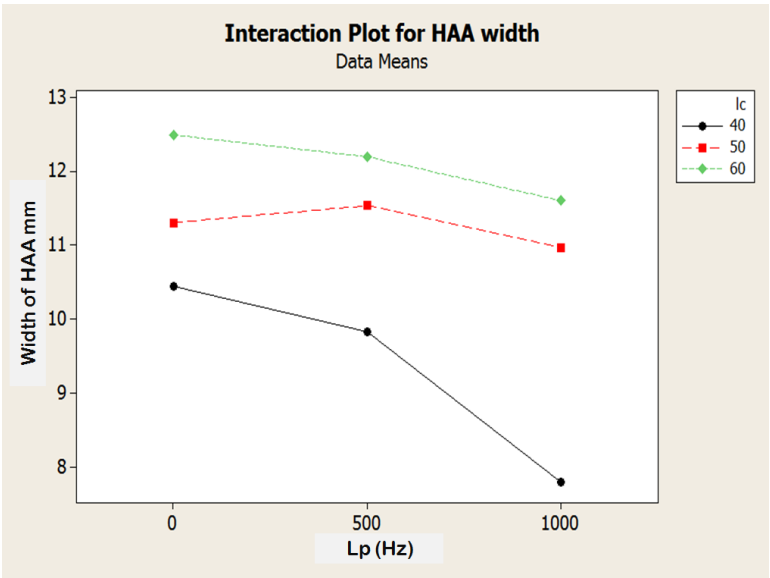

Figure 4.5 Interaction plot of Lp for HAA width

The oscillations of pulse current do not give a chance for the heat in the weld pool to separate and the head will be more concentrated in the fusion zone. The pulsed current welding includes many Metallurgical advantages such as refinement of

fusion zone grain size and substructure, reduced width of HAZ and control of segregation.

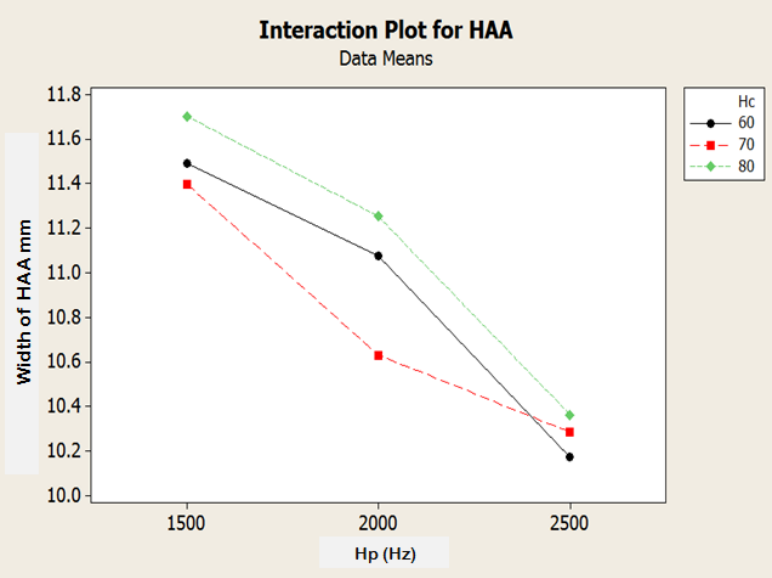

Figure 4.6 Interaction plot of Hp for HAA width

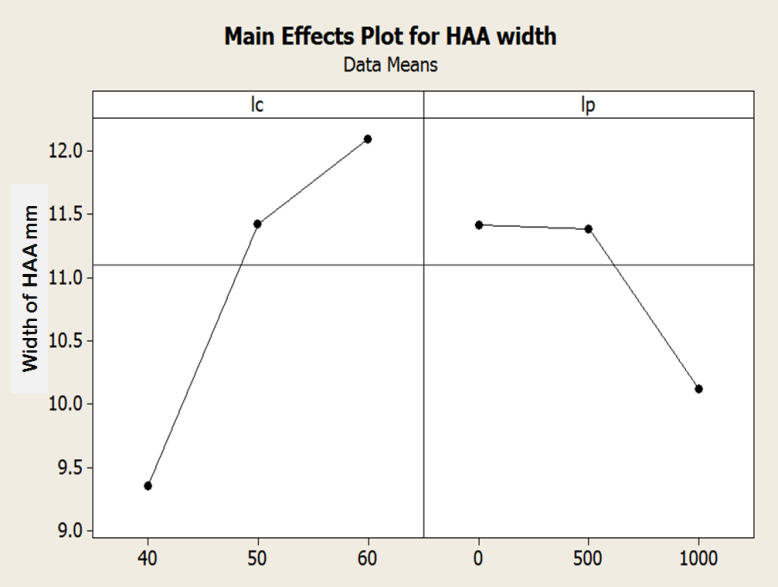

Figure 4.7 Main effects plot of Lp, Lc for HAA

Higher heat affected zone reduces the weld service life, the heat input should be harnessed to have a good penetration, the increasing of HAZ mean more heat input leads to more distortion so less heat input with full penetration will give sound welds.

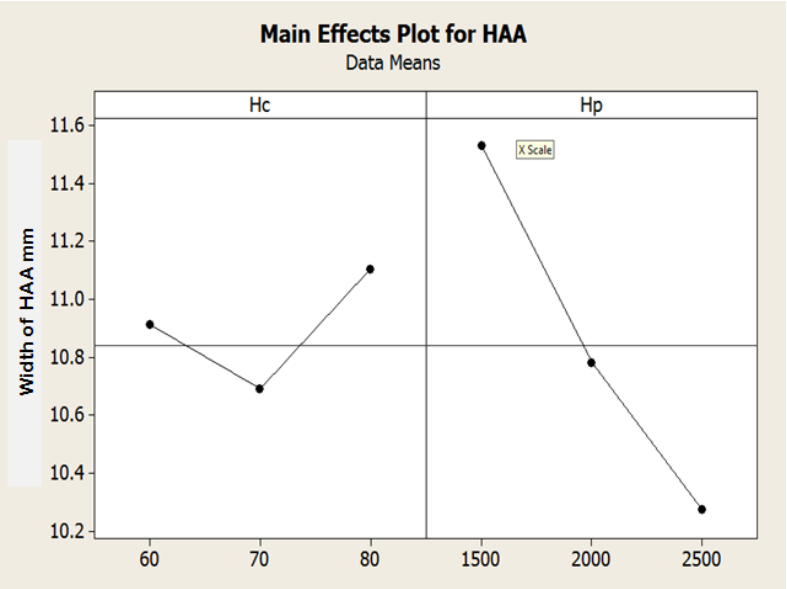

Figure 4.8 Main effects plot of Hp, Hc for HAA

4.3.3 Effects of TIG welding input parameters on Mh (HAZ)

The interaction plots for low and high pulses show stable increasing of micro hardness with the increasing of pulsing as shown in Figure 4.9, and 4.10. On the other hand the low current in the interaction plot of Lp for Mh (HAZ) shows higher hardness than high current in the interaction plot of Hp for Mh (HAZ) it is known that the increasing in current due to increasing in hardness, that means the pulsing with low current was more efficient because in low currents more grain refinement occurs as demonstrated in Figure 4.1. The martensitic structure has also increased the hardness of Ti-6AL-4V alloy.

The force that makes indentation will face many trammels while moving inside the metal, the grain boundaries have higher hardness than their grains and this leads to increasing of hardness.

Both the tensile test and hardness test measure the resistance of a metal to plastic flow, the hardness decreased with increasing grain size, increasing of grains number leads increasing of boundaries.

More clearly view can be obtained from Main effects plot of inputs for Mh (HAZ) as shown in Figure 4.11, and 4.12.

Figure 4.9 Interaction plot of Lp for Mh (HAZ)

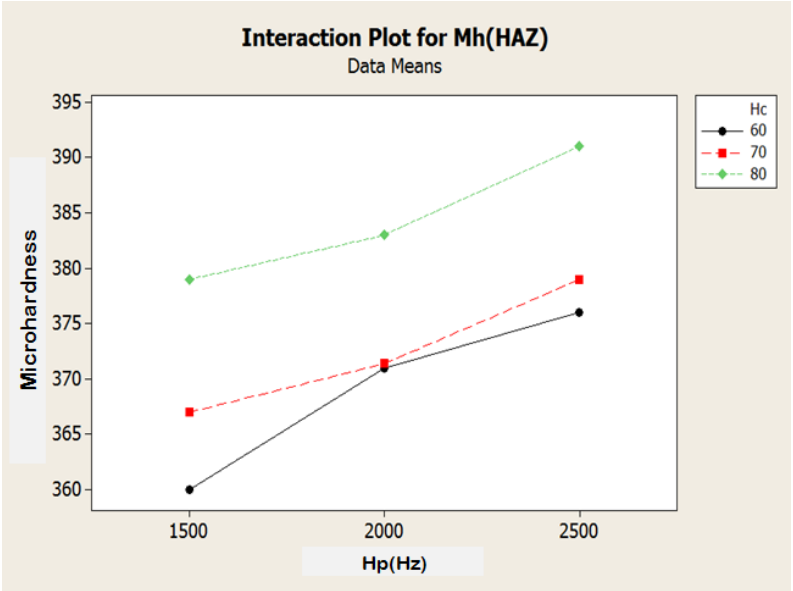

Figure 4.10 Interaction plot of Hp for Mh (HAZ)

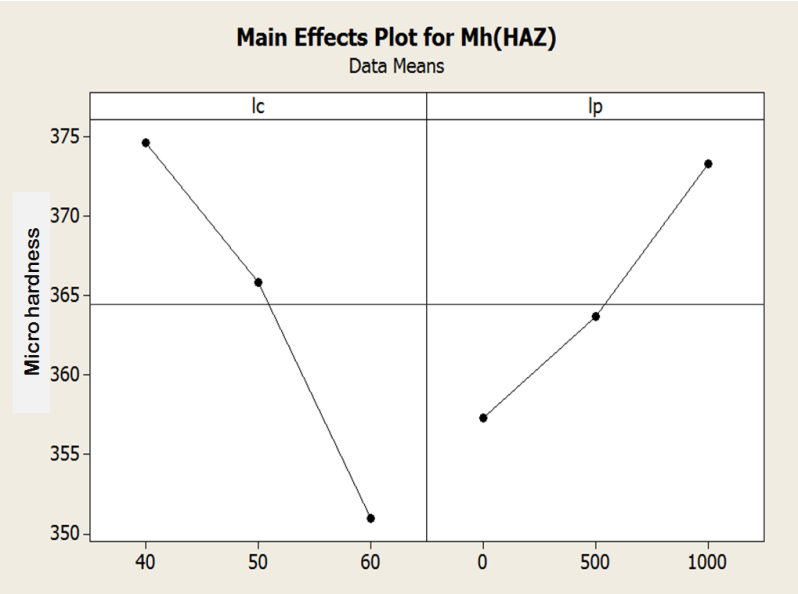

Figure 4.11 Main effects plot of Lp, Lc for Mh (HAZ)

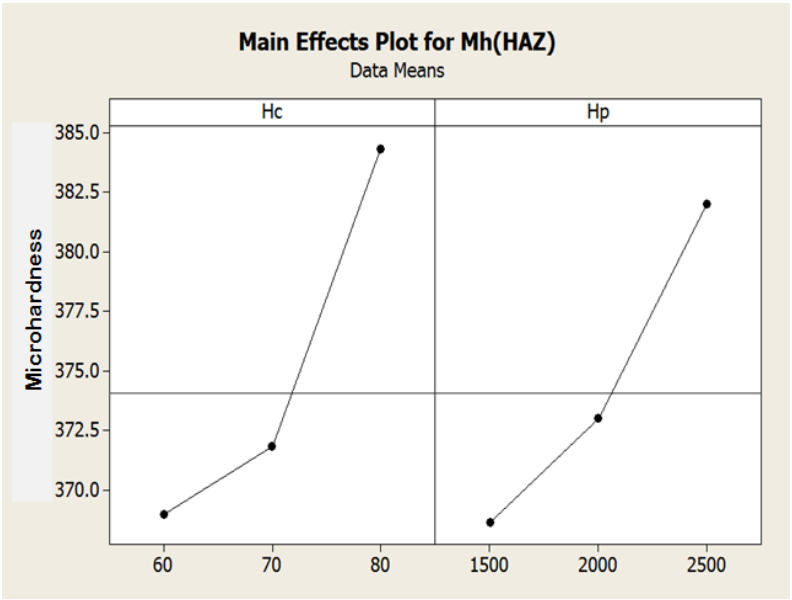

Figure 4.12 Main effects plot of Hp, Hc for Mh (HAZ)

4.3.4 Mathematical modeling of TIG welding

Scientists have devised many ways for the purpose of controlling the different properties of metals this work opens the field also to change some of mechanical properties and how to control them by using the equation that estimated from regression analyses. Regression analysis gives a high enough reliability accompanied by the regression equation. In this work ANOVA test was applied to all 26 experiments in order to find the important and unimportant factors. The regression

analysis results, R^2 and adjusted R^2 percentage values of the conducted test results are all given in Appendix B.

The regression analyses equation and R^2 and adjusted R^2 for Lc, Lp with Gs is:

$$Gs = 124380-1499Lc +12 Lp \quad (40 < Lc < 60), (0 < Lp < 1000) \qquad 4.1$$

$R^2 = 96.5\%$, adjusted $R^2 = 95.8\%$

The regression analyses equation and $R^2$and adjusted R^2 for Hc, Hp with Gs is:

$$Gs = 38372 – 1078 Hc + 55 Hp \quad (60 < Hc < 80), (1500 < Hp < 250) \qquad 4.2$$

$R^2 = 87.6\%$, adjusted $R^2 = 85.1\%$

The regression analyses equation and $R^2$and adjusted R^2 for Lc, Lp with HAA is:

$$HAA = 4.89 + 0.137 Lc – 0.00129 Lp \qquad 4.3$$

$R^2 = 78.9\%$, adjusted $R^2 = 74.7\%$

The regression analyses equation and $R^2$and adjusted R^2 for Hc, Hp with HAA is:

$$HAA = 12.7 + 0.00965 Hc – 0.00126 Hp \qquad 4.4$$

$R^2 = 82.8\%$, adjusted $R^2 = 79.3\%$

The regression analyses equation and $R^2$and adjusted R^2 for Lc, Lp with Mh (HAZ) is:

$$Mh (HAZ) = 416 – 1.18 Lc + 0.0160 Lp \qquad 4.5$$

$R^2 = 88.6\%$, adjusted $R^2 = 86.4\%$

The regression analyses equation and R^2 and adjusted R^2 for Hc, Hp with Mh (HAZ) is:

$$Mh (HAZ) = 294 + 0.767 Hc + 0.0133 Hp \qquad 4.6$$

$R^2 = 81.0\%$, adjusted $R^2 = 77.2\%$

CHAPTER 5

SUMMARY AND CONCLUSIONS

5.1 Summary and Conclusions

This work aims to investigate the effects of pulses and currents used in TIG welding technique on microstructure of Ti-6AL-4V alloy, which is practically used for aerospace applications and improve mechanical properties of Ti-6AL-4V. With the success of the work, an extensive experimental work was developed and conducted. The pulse value (0, 500, 1000, 1500, 2000, 2500) Hz, and current value (40, 50, 60, 70, 80) A, used in these experiments. The literature has been reviewed and the border for this work was determined. In order to assess the experiments correctly and accurately, an experimental set-up was prepared. The experiments were designed by statistical techniques and accurate measurements software and equipment were used.

Correlate the use of TIG welding pulse-current with microstructure and mechanical properties and obtain sound welds using well determined pulses-currents in TIG welding without welding defects was the primary objective of this work. To perform this task, statistical technique was used to generate experiments set-up, detect the relations of TIG welding process parameters with outputs. The results obtained from DOE–RS revealed that the responses or outputs can be used to improve Ti-6AL-4V microstructure and mechanical properties.

From the relations between TIG welding pulse, amperage parameters and the output. The following conclusions in this study can be outlined as follows;

- Lc, Hc, Lp and Hp were the main parameters that effects on Gs for all set of experiments. However, Gs were adversely affected by the increasing currents factor on Ti-6AL-4V alloy specimens, on the other hand pulsing works as positive factor where Gs is directly proportional to increasing in pulsing.

- HAA increased with the increasing of TIG welding current on the contrary with pulsing were the HAA decreases as the pulsing increased.

- Mh (HAZ) shows significant increasing of hardness with the increasing of pulsing, but inversely reacting with the increasing in currents.

5.2 Recommendation for Further Studies

Employment of the following points will be beneficial for extension of this study;

- Increasing the pulsing range by using more than six pulsing parameters, like to make the difference between the pulses 250Hz instead of 500Hz, and using more than two inputs like add pulse on time, and pulse off time.

- Study the effects of pulsing on mechanical properties of Ti-6AL-4V such as toughness, tensile strength and bending.

REFERENCES

[1] Sindo Kou. (2003). 2nd Edition Welding Metallurgy. Hoboken, New Jersey: *John Wiley & Sons, Inc*.

[2] Rowan K. Learya, Eleanor Mersonb, Keith Birminghamc, David Harveyc, Rik Brydson. (2010). Microstructural and Microtextural Analysis of InterPulse GTCAW Welds in Cp-Ti and Ti–6Al–4V, *Materials Science and Engineering **A***, **527**, 7694-7705.

[3] H. Liu, K. Nakata, N. Yamamoto, J. Liao. (2011). Microstructural Characteristics and Mechanical Properties in Laser Beam Welds of Ti6Al4V alloy, *J Mater Sci*,**47**, 1460-1470.

[4] M. Balasubramanian, V. Jayabalan, and V. Balasubramanian. (2008). Developing Mathematical Models to Predict Grain Size and Hardness of Argon Tungsten Pulse Current Arc Welded Titanium Alloy, *journal of materials processing technology*, **9 6**, 222–229.

[5] Yu Zhang, Yutaka S. Sato, Hiroyuki Kokawa, Seung Hwan C. Park, Satoshi Hirano. (2007). Microstructural Characteristics and Mechanical Properties of Ti–6Al–4V Friction Stir Welds, *Materials Science and Engineering **A***, **485**, 448–455.

[6] N. Kishore Babu , S. Ganesh Sundara Raman, R. Mythili, S. Saroja. (2006). Correlation of Microstructure With Mechanical Properties of TIG Weldments of Ti–6Al–4V Made with and without Current Pulsing, *Materials Characterization*, **58**, 581–587.

[7] V. Balasubramanian, V. Jayabalan, M. Balasubramanian. (2008). Effect of Current Pulsing on Tensile Properties of Titanium Alloy, *Materials and Design*, **29**, 1459–1466.

[8] osé A. Orlowski de Garcia, Gérson Luiz de Lima, Wilson D. Bocallão Pereira, Valdir Alves Guimarães, Carlos de Moura Neto, Ronaldo Pinheiro R. Paranhos. (2010). Characterization of Titanium Welded Joints by The Orbital Gas Tungsten Arc Welding Process for Aerospace Application, *Jatm*, **2**, 211-218.

[9] M. Balasubramanian, V. Jayabalan, V. Balaubramanian. (2007). Modeling Corrosion Behavior of Gas Tungsten Arc Welded Titanium Alloy, *Transactions of Nonferrous Metals Society of China*, **17,** 676-680.

[10] CLEMEX intelligent microscopy. (2009). Micro-Hardness Testing of Heat Affected Zones, Available at: http://ebookbrowse.com/clemex-cmt-pdf-d286347155. Accessed 16.8.2012.

[11]Hidetoshi Fujii, Toyoyuki Sato, Shanping Lu, Kiyoshi Nogi. (2007). Development of an Advanced A-TIG (AA-TIG) Welding Method by Control of Marangoni Convection, *Materials Science and Engineering* ***A***, **495**, 296–303.

[12] W. Bochnowski. (2012). Microstructure and Microhardness of Ti6Al4V Alloy Treated by GTAW SiC Alloying, *Polish Academy of Sciences*, **12,** 261 – 266.

[13] E. Akman, A. Demir, T. Canel, T. Sınmazc¸elik. (2008). Laser welding of Ti6Al4V Titanium Alloys, *journal of materials processing technology*, **2 0 9**, 3705-3713.

[14] Sicknan Soares da ROCHA,Gelson Luis ADABO, Guilherme Elias Pessanha HENRIQUES, Mauro Antônio de Arruda NÓBILO. (2006). Vickers Hardness of Cast Commercially Pure Titanium and Ti-6Al-4V Alloy Submitted to Heat Treatments, *Brazilian Dental Journal*, **17**, 126-129.

[15] N. Kishore Babu , S. Ganesh Sundara Raman, R. Mythili, S. Saroja. (2007) .Correlation of Microstructure with Mechanical Properties of TIG Weldments of Ti–6Al–4V made with and without current pulsing, *Materials Characterization*, **58**, 581–587.

[16] SUI Yan-wei,, LI Bang-sheng, LIU Ai-hui, NAN Hai, GUO Jing-jie, FU Heng-zhi. (2007). Microstructures and Hardness of Ti-6Al-4V Alloy Staging Castings Under Centrifugal Field, *Transactions of Nonferrous Metals Society of China*, **18,** 291-296.

[17] J. W. Elmer, T. A. Palmer, S. S. Babu, W. Zhang, T. DebRoy. (2003). Direct Observations of Phase Transitions in Ti-6Al-4V Alloy Transient Welds Using Time Resolved X-Ray Diffraction, *Journal of Applied Physics*, **51**, 1-46.

[18] Bernd Baufeld, Omer Van Der Biest, and Steven Dillien. (2010). Texture and Crystal Orientation in Ti-6Al-4V Builds Fabricated by Shaped Metal Deposition, *The Minerals, Metals & Materials Society and ASM International*, **41**, 1917-1927.

[19] Bupesh Raja V.K. , Palani Kumar K. , Elangovan K. , Manoharan N. (2009). Essects of Weldind Prosess on Microstructure of Ti6Al4V Weldments**,** *International Journal on Design and Manufacturing Technologies*, **3**, 12-18.

[20] M. Balasubramanian, V. Jayabalan, V. Balasubramanian. (2009). Effect of Pulsed Current Gas Tungsten Arc Welding Parameters on Microstructure of Titanium Alloy Welds, *Journal of Manufacturing Science and Engineering*, **131**, 1-4.

[21] M. Balasubramanian, V. Jayabalan, and V. Balasubramanian. (2008). Prediction and Optimization of Pulsed Current Gas Tungsten Arc Welding Process Parameters to Obtain Sound Weld Pool Geometry in Titanium Alloy Using Lexicographic Method, *ASM International*, **18**, 871–877.

[22] M. Balasubramanian, V. Jayabalan, and V. Balasubramanian. (2008). Effect of Pulsed Gas Tungsten Arc Welding on Corrosion Behavior of Ti–6Al–4V Titanium Alloy, *Materials& Design*, **29**, 1359–1363.

[23] A. Traidia, F.Roger, E. Guyot. (2010). Optimal Parameters for Pulsed Gas Tungsten Arc Welding in Partially and Fully Penetrated Weld Pools**,** *International Journal of Thermal Sciences*, **49**, 1197-1208.

[24] Tadayuki OTANI. (2007). Titanium Welding Technology, *Nippon Steel Technical Report*, **95**, 88-92.

[25] R Leary, E Merson and R Brydson. (2010). Microtextures and Grain Boundary Misorientation Distributions in Controlled Heat Input Titanium Alloy Fusion Welds, *I0p science*, **241**, 1-4.

[26] M. Balasubramanian, V. Jayabalan, and V. Balasubramanian. (2008). The Response Surface Approach of Optimising the Pulsed-Current Gas Tungsten Arc Welding Parameters to Attain Maximum Impact Toughness, *Int. J. Microstructure and Materials Properties*, **3**, 823-835.

[27] M. Balasubramanian, V. Jayabalan, and V. Balasubramanian. (2007). Optimizing the Pulsed Current GTAW Parameters to Attain Maximum Impact Toughness, *Taylor & Francis Materials and Manufacturing Processes*, **23**, 69–73.

[28] M. Balasubramanian & V. Jayabalan V. Balasubramanian. (2007). Optimizing Pulsed Current Parameters to Minimize Corrosionrate in Gas Tungsten Arc Welded Titanium Alloy, *Int J Adv Manuf Technol*, **39**, 474-481.

[29] A.C.Davies. (1993). the Science and Practice of Welding, Volume 2, the Pitt Building, Trumpington Street, Cambridge, United Kingdom: The Press Syndicate of the University of Cambridge.

[30] Miller welds.2011. TIG Handbook for GTAW Technical guide, Available at: http://www.millerwelds.com/resources/TIGhandbook/. Accessed 20.6.2012

[31] AZoM.com the A to Z of Materials.2011.Titanium - Welding and Heat Treating, Available at: http://www.azom.com/article.aspx?ArticleID=1245. Accessed 20.6.2012.

[32] Matthew J. Donachie, Jr. (2000). Titanium: A Technical Guide, 2nd edition. ASM International. United States of America: ASM International.

[33] ASM Handbook Committee. (1985). Metallography and Microstructures ASM Handbook, volume 9. United States of America: ASM International.

[34] ASTM International. (2012). E112 -10 Standard Test Methods for Determining Average Grain Size, United States: ASTM International

[35] Harry Chandler. (1999). Introduction to Hardness Testing, 2nd Edition, United States: ASTM International

[36] MINITAB User's Manual. (2010). Release 16.0. Documentation for MINITAB.

APPENDICES

Appendix A: Microscope Pictures for Gs

Appendix B: Mathematical Modeling TIG Welding Input Parameters

Appendix A

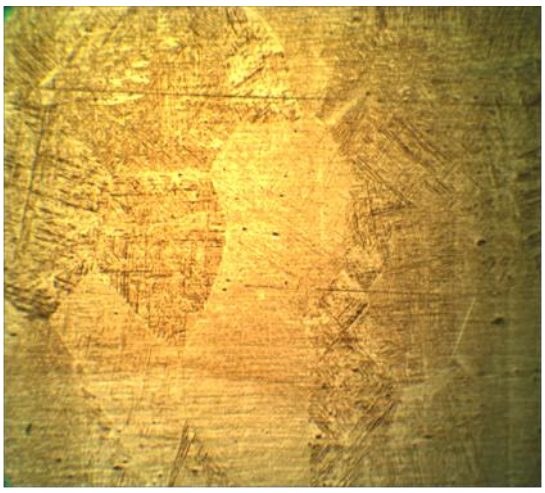

Figure A1. L1: 40A, 1000Hz

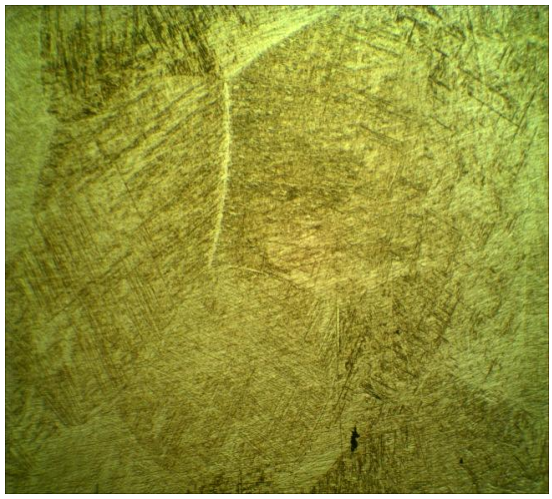

Figure A2. L2: 60A, 500Hz

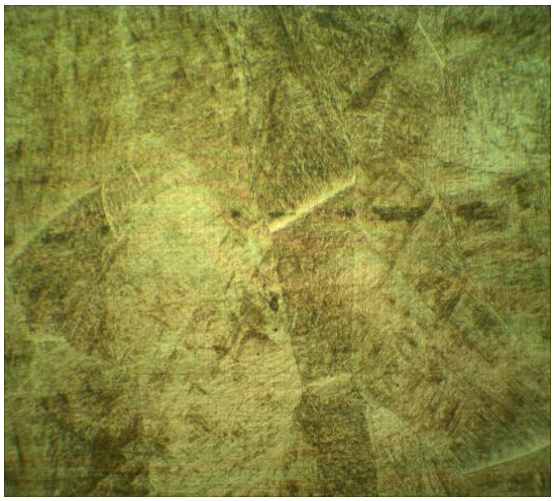

Figure A3. L3: 50A, 500Hz

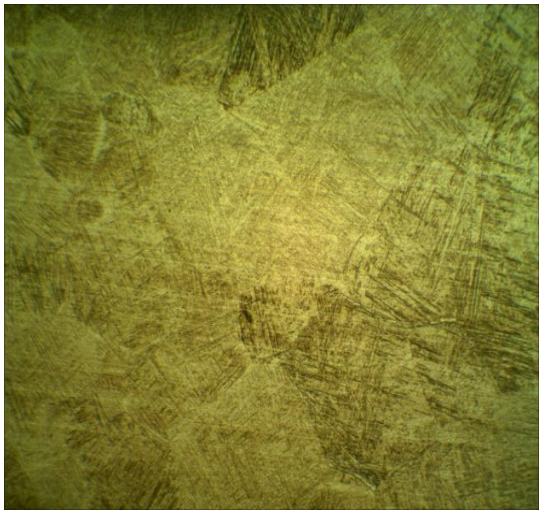

Figure A4. L4: 40A, 500Hz

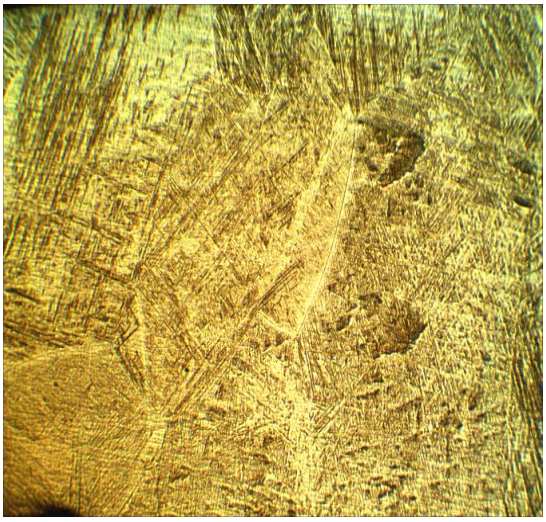

Figure A5. L5: 50A, 0Hz

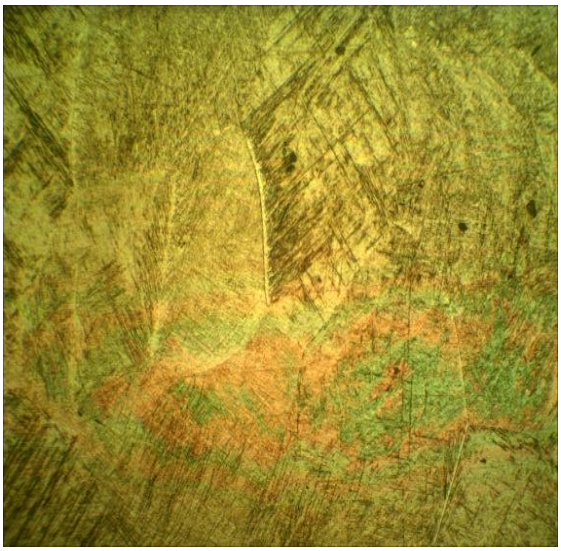

Figure A6. L6: 50A, 500Hz

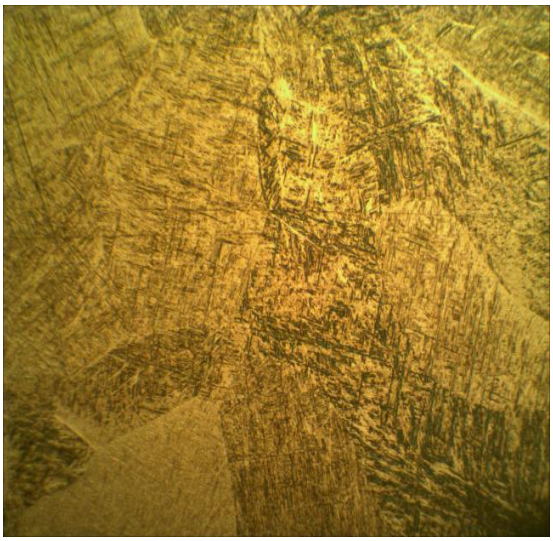

Figure A7. L7: 60A, 1000Hz

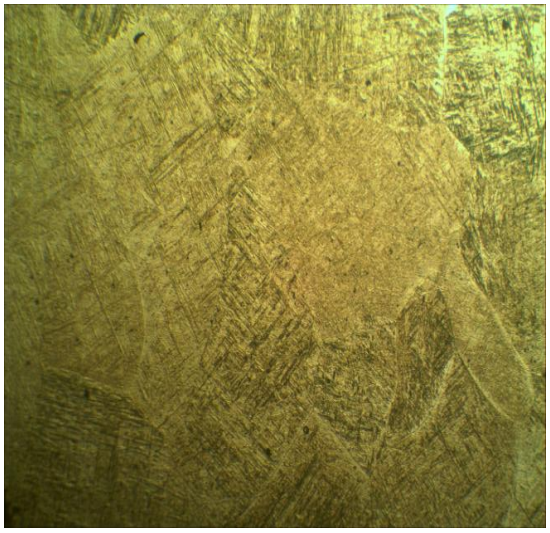

Figure A8. L8: 40A, 0Hz

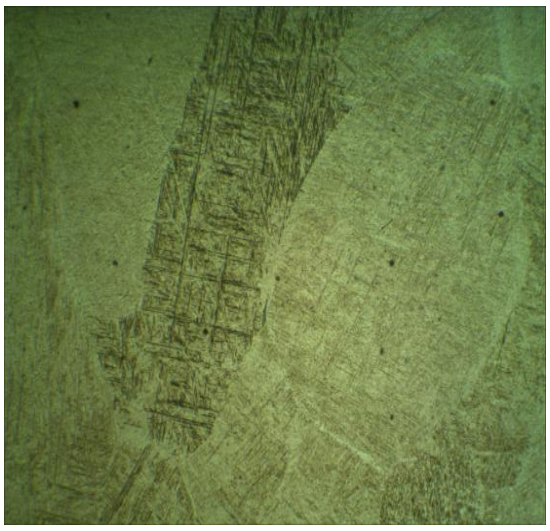

Figure A9. L9: 50A, 500Hz

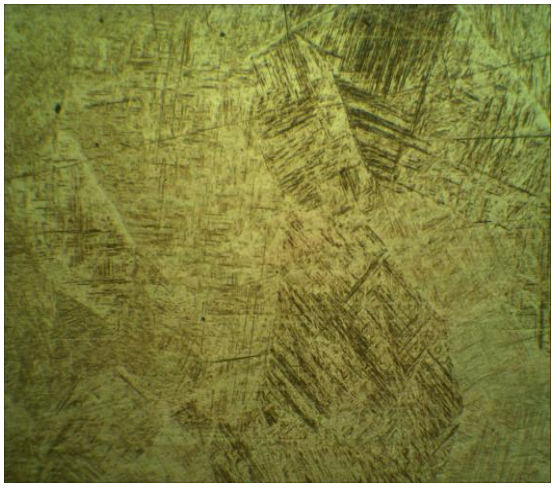

Figure A10. L10: 50A, 500Hz

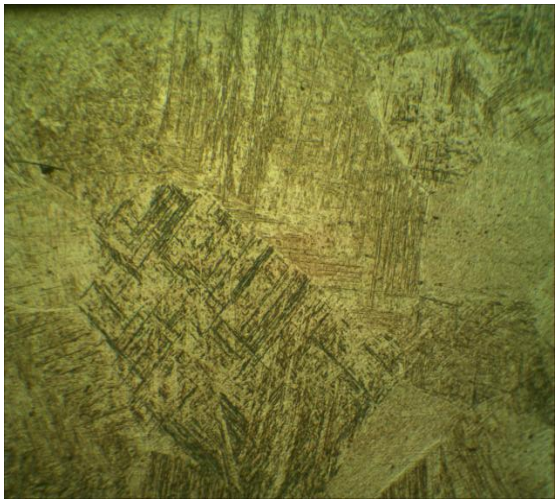

Figure A11. L11:60A, 0HZ

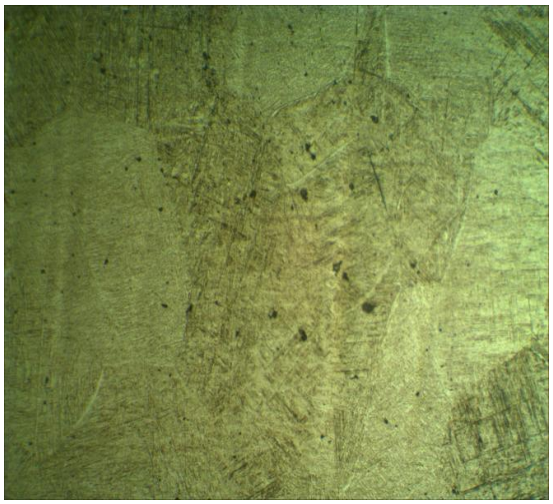

Figure A12. L12: 50A, 1000Hz

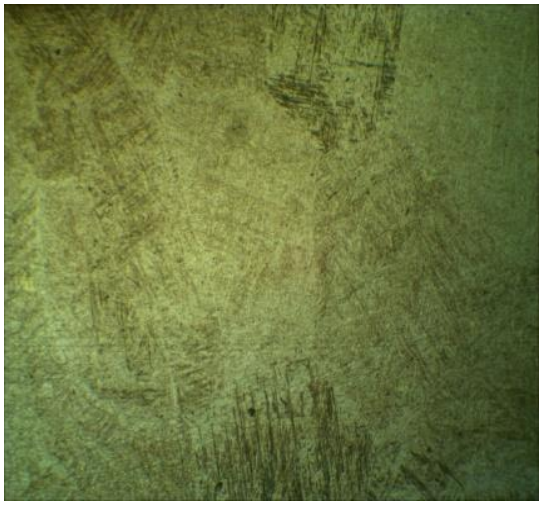

Figure A13. L13:50A, 500Hz

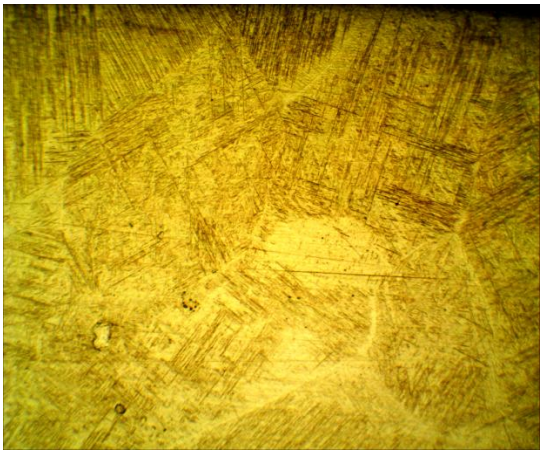

Figure A14. H1: 60A, 1500Hz

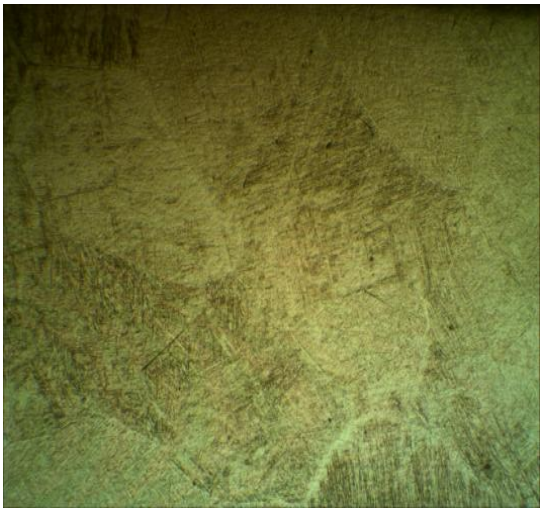

Figure A15. H2: 70A, 2000Hz

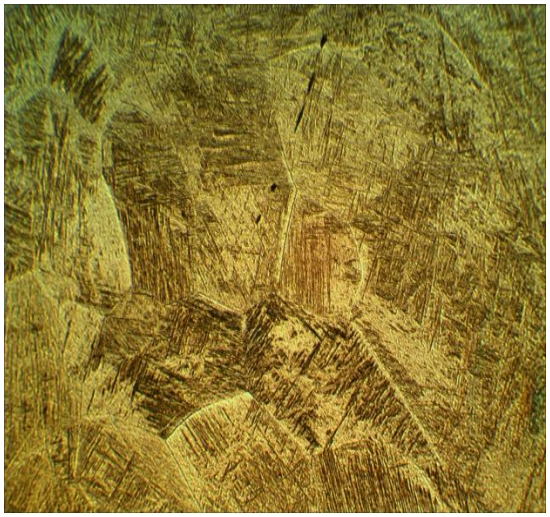

Figure A16. H3: 80A, 2500Hz

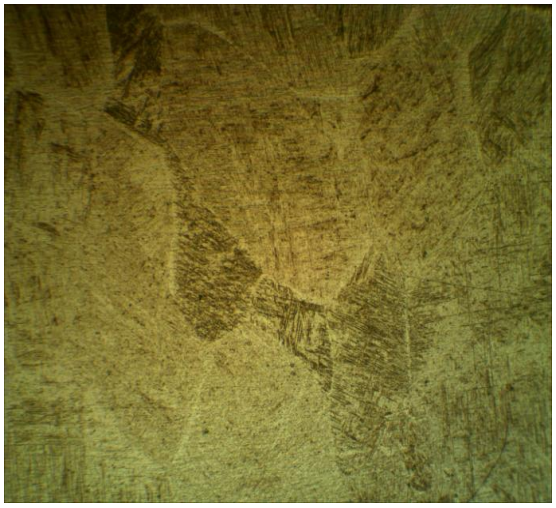

Figure A17. H4:60A, 2500Hz

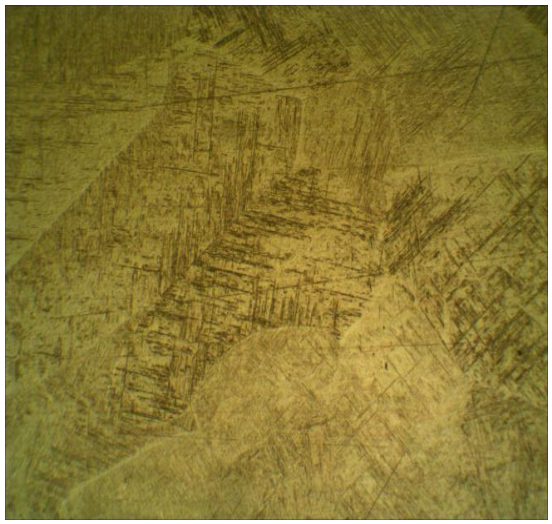

Figure A18. H5:80A, 2000Hz

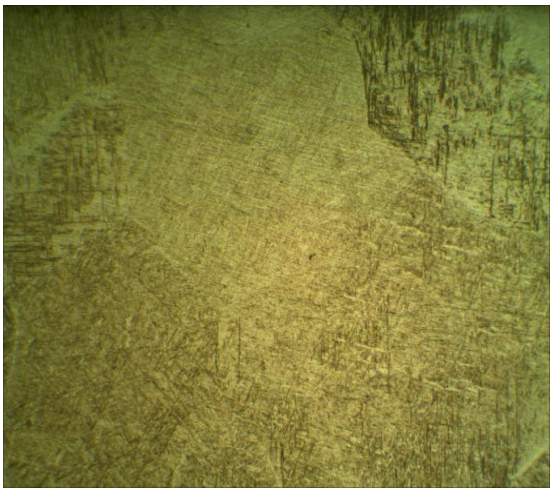

Figure A19. H6: 70A, 2500Hz

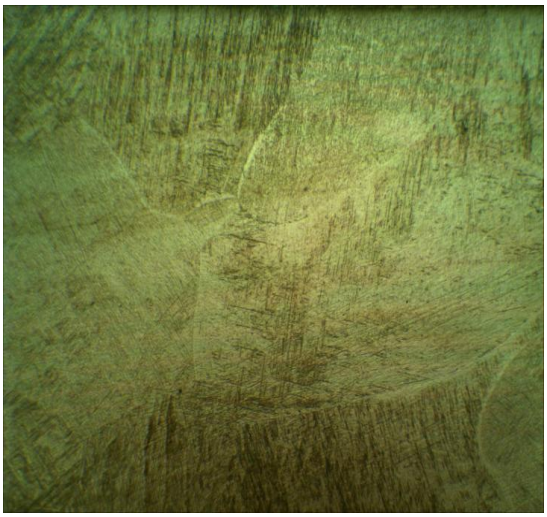

Figure A20. H7: 60A,2000Hz

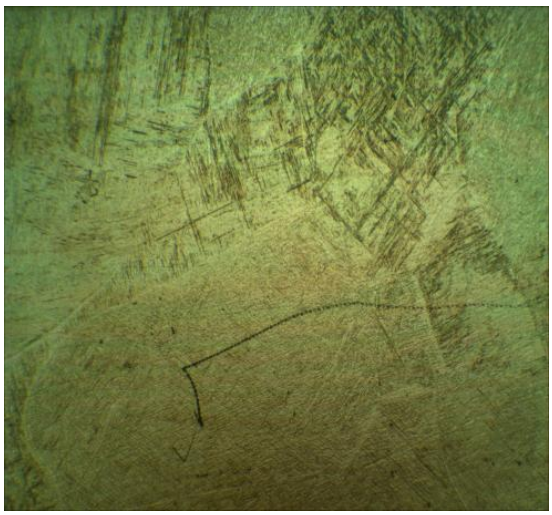

Figure A21. H8: 80A, 1500Hz

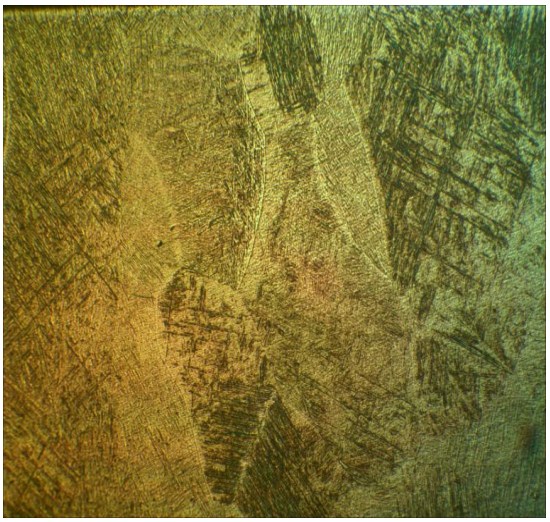

Figure A22. H9: 70A, 2000Hz

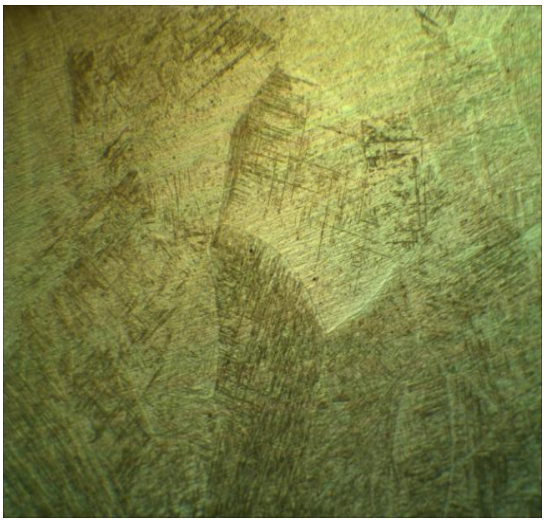

Figure A23. H10: 70A, 2000Hz

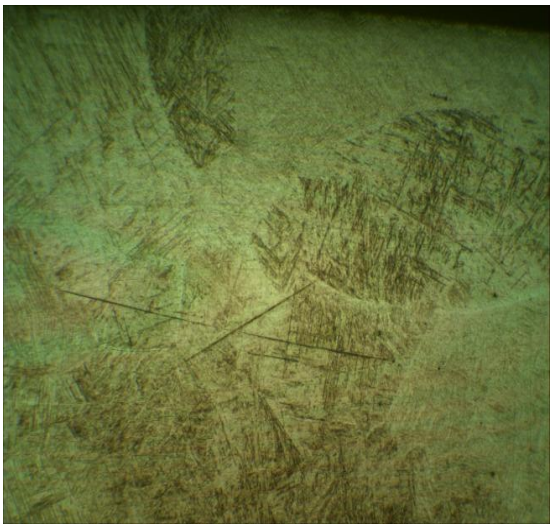

Figure A24. H11: 70A, 1500Hz

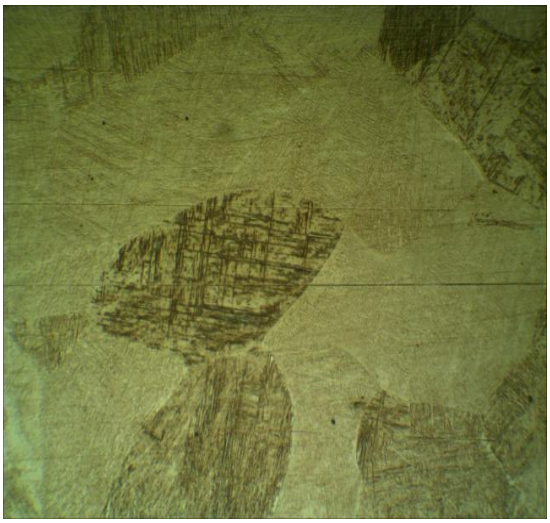

Figure A25. H12: 70A, 2000Hz

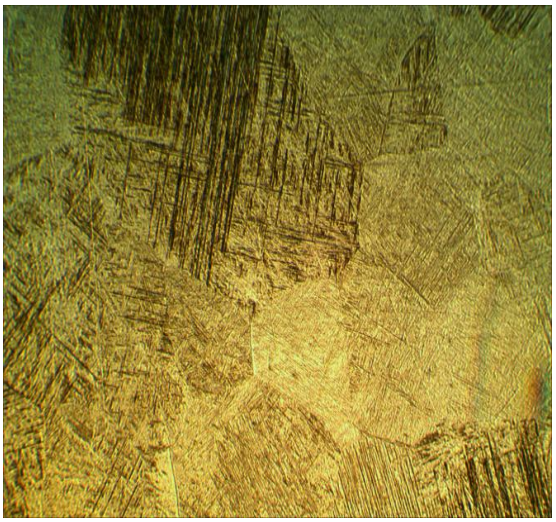

Figure A26. H13: 70A, 2000Hz

Appendix B

Table B1 Regression analyses for Lc, Lp with Gs

Regression Analysis: Gs versus lc, lp

The regression equation is
Gs = 124380 - 1499 lc + 12.0 lp

Predictor	Coef	SE Coef	T	P
Constant	124380	5021	24.77	0.000
lc	-1499.35	97.61	-15.36	0.000
lp	11.993	1.952	6.14	0.000

S = 2390.92 R-Sq = 96.5% R-Sq(adj) = 95.8%

Analysis of Variance

Source	DF	SS	MS	F	P
Regression	2	1564575155	782287578	136.85	0.000
Residual Error	10	57164978	5716498		
Total	12	1621740133			

Source	DF	Seq SS
lc	1	1348838902
lp	1	215736253

Unusual Observations

Obs	lc	Gs	Fit	SE Fit	Residual	St Resid
7	60.0	42526	46411	1531	-3885	-2.12R

R denotes an observation with a large standardized residual.

Table B2 Regression analyses for Hc, Hp with Gs

Regression Analysis: Gs versus Hc, Hp

The regression equation is
Gs = 38372 - 1078 Hc + 55.0 Hp

Predictor	Coef	SE Coef	T	P
Constant	38372	28475	1.35	0.208
Hc	-1078.2	351.9	-3.06	0.012
Hp	55.023	7.039	7.82	0.000

S = 8620.83 R-Sq = 87.6% R-Sq(adj) = 85.1%

Analysis of Variance

Source	DF	SS	MS	F	P
Regression	2	5238754446	2619377223	35.25	0.000
Residual Error	10	743186828	74318683		
Total	12	5981941274			

Source	DF	Seq SS
Hc	1	697480266
Hp	1	4541274180

Table B3 Regression analyses for Lc, Lp with HAA width

Regression Analysis: HAA width versus lc, lp

The regression equation is
HAA width = 4.89 + 0.137 lc - 0.00129 lp

Predictor	Coef	SE Coef	T	P
Constant	4.893	1.275	3.84	0.003
lc	0.13710	0.02479	5.53	0.000
lp	-0.0012907	0.0004959	-2.60	0.026

S = 0.607339 R-Sq = 78.9% R-Sq(adj) = 74.7%

Analysis of Variance

Source	DF	SS	MS	F	P
Regression	2	13.7766	6.8883	18.67	0.000
Residual Error	10	3.6886	0.3689		
Total	12	17.4652			

Source	DF	Seq SS
lc	1	11.2778
lp	1	2.4987

Unusual Observations

Obs	lc	HAA width	Fit	SE Fit	Residual	St Resid
1	40.0	7.800	9.086	0.389	-1.286	-2.76R

R denotes an observation with a large standardized residual.

Table B4 Regression analyses for Hc, Hp with HAA width

Regression Analysis: HAA versus Hc, Hp

The regression equation is
HAA = 12.7 + 0.00965 Hc - 0.00126 Hp

Predictor	Coef	SE Coef	T	P
Constant	12.6754	0.7413	17.10	0.000
Hc	0.009650	0.009163	1.05	0.317
Hp	-0.0012560	0.0001833	-6.85	0.000

S = 0.224438 R-Sq = 82.8% R-Sq(adj) = 79.3%

Analysis of Variance

Source	DF	SS	MS	F	P
Regression	2	2.4222	1.2111	24.04	0.000
Residual Error	10	0.5037	0.0504		
Total	12	2.9259			

Source	DF	Seq SS
Hc	1	0.0559
Hp	1	2.3663

Table B5 Regression analyses for Lc, Lp with Mh (HAZ)

Regression Analysis: Mh(HAZ) versus lc, lp

The regression equation is
Mh(HAZ) = 416 - 1.18 lc + 0.0160 lp

Predictor	Coef	SE Coef	T	P
Constant	415.628	8.323	49.94	0.000
lc	-1.1833	0.1618	-7.31	0.000
lp	0.016000	0.003236	4.94	0.001

S = 3.96313 R-Sq = 88.6% R-Sq(adj) = 86.4%

Analysis of Variance

Source	DF	SS	MS	F	P
Regression	2	1224.17	612.08	38.97	0.000
Residual Error	10	157.06	15.71		
Total	12	1381.23			

Source	DF	Seq SS
lc	1	840.17
lp	1	384.00

Table B6 Regression analyses for Hc, Hp with Mh (HAZ)

Regression Analysis: Mh(HAZ) versus Hc, Hp

The regression equation is
Mh(HAZ) = 294 + 0.767 Hc + 0.0133 Hp

Predictor	Coef	SE Coef	T	P
Constant	293.74	12.60	23.31	0.000
Hc	0.7667	0.1558	4.92	0.001
Hp	0.013333	0.003115	4.28	0.002

S = 3.81562 R-Sq = 81.0% R-Sq(adj) = 77.2%

Analysis of Variance

Source	DF	SS	MS	F	P
Regression	2	619.33	309.67	21.27	0.000
Residual Error	10	145.59	14.56		
Total	12	764.92			

Source	DF	Seq SS
Hc	1	352.67
Hp	1	266.67